Applied Geochemistry xxx (2012) xxx–xxx

Contents lists available at SciVerse ScienceDirect

Applied Geochemistry

journal homepage: www.elsevier.com/locate/apgeochem

Metal partitioning in sediments and mineralogical controls on the acid mine drainage in Ribeira da Água Forte (Aljustrel, Iberian Pyrite Belt, Southern Portugal)

Flávia Maia [a,1], Cláudia Pinto [a], João Carlos Waerenborgh [b], Mário A. Gonçalves [a,c,*], Cátia Prazeres [a,2], Ondina Carreira [a], Susana Sério [b,d]

[a] Departamento de Geologia, Faculdade de Ciências da Universidade de Lisboa, Ed. C6 piso 4, Campo Grande, 1749-016 Lisboa, Portugal
[b] Instituto Tecnológico e Nuclear, Instituto Superior Técnico, Universidade Técnica de Lisboa, CFMC-UL, EN 10, 2686-953 Sacavém, Portugal
[c] CREMINER/LARSyS, Faculdade de Ciências da Universidade de Lisboa, Ed C6 piso 3, Campo Grande, 1749-016 Lisboa, Portugal
[d] CEFITEC, Departamento de Física, Faculdade de Ciências e Tecnologia da Universidade Nova de Lisboa, 2829-516 Caparica, Portugal

ARTICLE INFO

Article history:
Received 3 April 2011
Accepted 28 February 2012
Available online xxxx
Editorial handling by R. Seal II

ABSTRACT

This work focuses on the geochemical processes taking place in the acid drainage in the Ribeira da Água Forte, located in the Aljustrel mining area in the Iberian Pyrite Belt. The approach involved water and stream sediment geochemical analyses, as well as other techniques such as sequential extraction, Mössbauer spectroscopy, and X-ray diffraction. Ribeira da Água Forte is a stream that drains the area of the old mine dumps of the Aljustrel mine, which have for decades been a source of acid waters. This stream flows to the north for a little over than 10 km, but mixes with a reduced, organic-rich, high pH waste water from the municipal waste water pools of the village. This water input produces two different results in the chemistry of the stream depending upon the season: (i) in the winter season, effective water mixing takes place, and the flux of acid water from the mine dumps is continuous, resulting in the immediate precipitation of the Fe from the acid waters; (ii) during the summer season, acid drainage is interrupted and only the waste water feeds the stream, resulting in the reductive dissolution of Fe hydroxides and hydroxysulfates in the stream sediments, releasing significant quantities of metals into solution. Throughout the year, water pH stays invariably within 4.0–4.5 for several meters downstream of this mixing zone even when the source waters come from the waste water pools, which have a pH around 8.4. The coupled interplay of dissolution and precipitation of the secondary minerals (hydroxides and sulfates), keeps the system pH between 3.9 and 4.5 all along the stream. In particular, evidence suggests that schwertmannite may be precipitating and later decomposing into Fe hydroxides to sustain the stream water pH at those levels. While Fe content decreases by 50% from solution, the most important trace metals are only slightly attenuated before the solution mixes with the Ribeira do Rôxo stream waters. Concentrations of As are the only ones effectively reduced along the flow path. Partitioning of Cu, Zn and Pb in the contaminated sediments also showed different behavior. Specific/non-specific adsorption is relevant for Cu and Zn in the upstream branch of Ribeira da Água Forte with acid drainage conditions, whereas the mixture with the waste water causes that the association of these metals with oxyhydroxide to be more important. Metals bound to oxyhydroxides are on the order of 60–70% for Pb, 50% for Cu and 30–60% for Zn. Organic matter is only marginally important around the waste water input area showing 2–8% Cu bound to this phase. These results also show that, although the mixing process of both acid and organic-rich waters can suppress and briefly mitigate some adverse effects of acid drainage, the continuing discharge of these waste waters into a dry stream promotes the remobilization of metals fixed in the secondary solid phases in the stream bed back into solution, a situation that can hardly be amended back to its original state.

1. Introduction

The Iberian Pyrite Belt (IPB) has a long mining history that has resulted in several abandoned mines currently causing severe environmental problems related to metal pollution. The large accumulation of mine wastes with minimal or no treatment results in the development of acid-mine drainage (AMD), which is a major contamination source for groundwater, streams and rivers, soils,

* Corresponding author at: Departamento de Geologia, Faculdade de Ciências da Universidade de Lisboa, Ed. C6 piso 4, Campo Grande, 1749-016 Lisboa, Portugal.
E-mail address: mgoncalves@fc.ul.pt (M.A. Gonçalves).
[1] Present address: Amphos21 Consulting S.L., Passeig de García i Faria, 49-51, E08019 Barcelona, Spain.
[2] Present address: Laboratório Nacional de Energia e Geologia, Estrada da Portela, Bairro do Zambujal, Alfragide, 2611-901 Amadora, Portugal.

0883-2927/$ - see front matter © 2012 Elsevier Ltd. All rights reserved.
http://dx.doi.org/10.1016/j.apgeochem.2012.02.036

and sediments. AMD results from a process triggered by pyrite oxidation, mostly aided by bacterial activity, producing acid waters with pH around 2 or less, abundant colloidal Fe and high concentrations of transition metals, which were important constituents in the exploited ores. A significant number of papers have described this problem in the IPB, the majority of which have been on the Spanish side of the IPB (Galán et al., 2003; Sánchez-España et al., 2005, 2008; Pérez-López et al., 2007, 2010; Hubbard et al., 2009), largely because of the exposure of the mineralization and common use of open-pit mining methods. The motivation for these studies arose from the large tailings spill and associated AMD that affected the Donaña National Park (Grimalt et al., 1999; Tovar-Sanchez et al., 2006). In either case, all mining operations handled massive amounts of waste rock that accumulated on the surface, some near important populated areas and villages, such as Aljustrel. These waste rock-piles, subjected to weathering, become significant sources of acid-mine waters that rapidly disperse into the drainage basin. AMD around Aljustrel has been a serious problem that affects several streams and results from decades of mining with little regard for the environment. Most of the evidence of environmental impact is still detectable in stream sediments but ongoing remediation and better mining practices have reduced the spread of acid drainage to many of these streams. However, Ribeira da Água Forte has remained an exception, mostly because it receives drainage from mine dumps, old cementation pools, and the acid–water pond that forms in the tailings site. Even though the land has been subjected to reclamation in recent years with the construction of water-diversion systems that tend to minimize waste rock–water interactions, the truth is that the major problems in the streams are far from being mitigated. Studying AMD systems is a challenging task because of the chemical complexity of acid-mine waters and their interaction with stream sediments, which includes the formation of secondary solid phases. This work focuses on a specific situation where acid-mine waters flowing along the Ribeira da Água Forte are mixed with reduced, organic-rich, high pH, waste waters in their path. Whereas the immediate effects result in the rapid neutralization of the AMD waters, this neutralizing capacity does not last for long, and the waters readily return to a low pH around 4.0–4.5 within the next hundreds of meters downstream. The situation does not vary much seasonally, even in the drier season when the water flowing from the mine wastes is temporarily interrupted. In order to understand this geochemical system and its potential attenuation effects, a survey of the mineralogy and metal partitioning among different phases in the stream sediments was performed using X-ray diffraction, Mössbauer spectroscopy, and sequential extraction techniques.

Generation of acid-mine waters is known to be mostly due to pyrite oxidation (e.g. Nordstrom and Southam, 1997; Nordstrom and Alpers, 1999; Druschel et al., 2005), even if pyrite is only a minor disseminated phase in the rock. The mechanisms that promote pyrite oxidation are generally described by

$$FeS_2 + 3.5O_2 + H_2O = Fe^{2+} + 2SO_4^{2-} + 2H^+ \quad (1)$$

and

$$FeS_2 + 14Fe^{3+} + 8H_2O = 15Fe^{2+} + 2SO_4^{2-} + 16H^+. \quad (2)$$

Reactions (1) and (2) reflect two oxidation mechanisms where either atmospheric O_2 or Fe^{3+} acts as the oxidant. It has been widely demonstrated that reaction (2) is much faster and more important (e.g., Nordstrom and Southam, 1997; Nordstrom and Alpers, 1999; and references therein), but is limited by the rate of Fe^{2+} oxidation. This oxidation step is the cornerstone of the whole process and outlines the importance of Fe-oxidizing bacteria in re-oxidizing the Fe^{2+} produced in reaction (2), as opposed to the sluggish process of O_2 diffusion towards the pyrite surface needed to produce the same effect abiotically (Nordstrom and Southam, 1997). The resulting highly acidic solution from reaction (2) also maintains the necessary conditions to keep Fe^{3+} dissolved, at least at the mineral surface (Bigham and Nordstrom, 2000). However this only describes the initial steps of AMD development, and the fate of reaction products, namely Fe^{2+} and SO_4^{2-} is crucial to understand the chemistry of both acid waters and stream sediments affected by the continuous flow of acid-mine waters for tens of kilometers. High Fe—SO_4^{2-} waters can be supersaturated with respect to various sulfates, including jarosite and schwertmannite (Bigham and Nordstrom, 2000). Ever since schwertmannite was first described (Bigham et al., 1994), its importance has been increasingly recognized in controlling the fate of trace metals and maintaining acid conditions (Acero et al., 2006; Knorr and Blodau, 2007; Peretyazhko et al., 2009). However, its proper recognition is significantly hindered because it is normally poorly crystallized, it is metastable, and it occurs commonly mixed with other nano-scale Fe-bearing phases, especially poorly crystalline Fe oxyhydroxides (Bigham and Nordstrom, 2000). Demonstrating the importance of these mechanisms and which other mechanisms are operative in these systems, requires an integrated approach to decipher not only the mineralogy, but also the chemistry of waters and stream sediments, and with which phases the metals in the sediment are associated.

Sequential extraction techniques are helpful to address this latter problem by providing an approximate picture on metal distribution within sediments. These techniques have been widely used as a way to quantify metal partitioning in different solid phases, allowing a better understanding of the behavior of metals in relation to their solubility, mobilization, and availability in several environments (Morillo et al., 2002; Pérez-López et al., 2008). This approach is never fully accurate because it is well known that sequential extraction techniques have several shortcomings, which include nonspecificity of extractants and re-adsorption of metals into other phases (Kheboian and Bauer, 1987; Bermond, 2001). Additionally, the use of conventional sequential extraction procedures published in the literature is inadequate for sediments from AMD environments, especially because of the large amounts of Fe oxyhydroxides. Therefore, a modified sequential extraction scheme is proposed. The pioneering work of Tessier et al. (1979) triggered a wealth of applications based on their method in spite of the recognized shortcomings, which have been hotly debated in the scientific literature. These limitations led to the proposal of alternative methods, some with the aim of being standard reference methods to be used by the scientific community (Quevauviller et al., 1994; Sahuquillo et al., 1999). However, this goal remains unrealized because there is not a single method that can be equally applied to all kinds of samples. In a much more modest perspective, several authors have tried to introduce modifications specially designed to meet their own requirements (e.g., Hirner, 1992, 1996; Breward et al., 1996). This customization was the objective in the present work and was achieved by incorporating the modifications proposed by Hirner (1996) and Breward et al. (1996), and inverting the sequence between the Fe oxyhydroxides and organic matter steps. This modification is justified by the large amount of Fe oxyhydroxides present in the samples together with reduced solid phases, mostly sulfides, that are easily oxidized and dissolved during the organic matter step.

2. Geological setting

The study area is located in the Aljustrel mining region, which belongs to the IPB (Fig. 1), and comprises six massive sulfide deposits within an approximate area of 12 km^2 totalling 250 Mt

Please cite this article in press as: Maia, F., et al. Metal partitioning in sediments and mineralogical controls on the acid mine drainage in Ribeira da Água Forte (Aljustrel, Iberian Pyrite Belt, Southern Portugal). Appl. Geochem. (2012), http://dx.doi.org/10.1016/j.apgeochem.2012.02.036

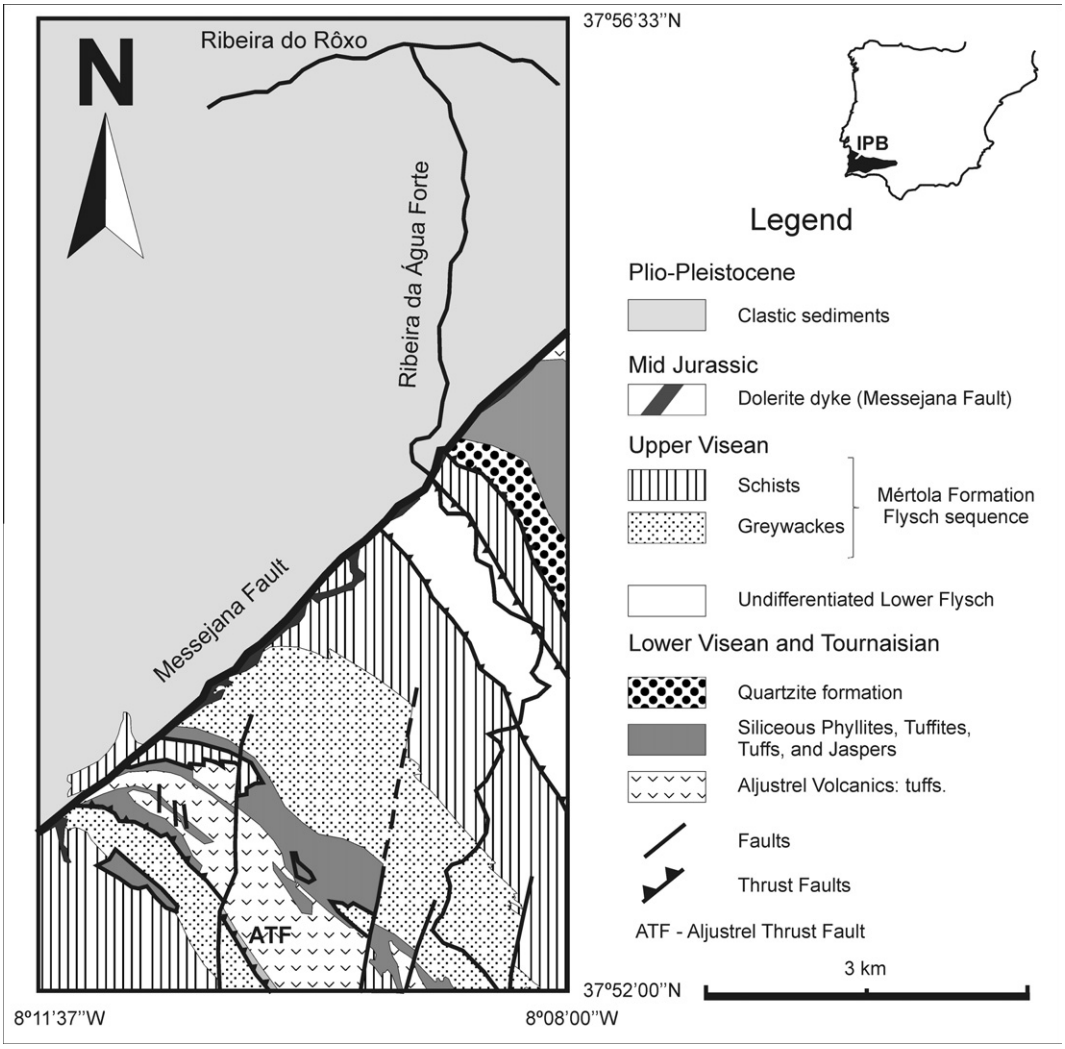

Fig. 1. Simplified geological map of the Aljustrel area (adapted from Schermerhorn et al. (1987)). The inset shows the Iberian Peninsula and the location of the Iberian Pyrite Belt (IPB).

of reserves and putting it amongst the most important massive sulfide deposits of the world (Carvalho, 1976; Barriga and Carvalho, 1983; Carvalho et al., 1999). The main rocks cropping out in the Aljustrel area are volcanic rocks, mostly rhyolites, covered by chemical sediments, which include jasper, constituting the so called volcanic–siliceous complex (upper Devonian–lower Visean) (Carvalho, 1976; Barriga and Carvalho, 1983; Barriga and Fyfe, 1998). This complex overlies the more recent lithologies belonging to the flysch group, an alternating sequence of schists and greywackes (upper Visean), along its SE border, which is marked by the major Aljustrel thrust fault (Oliveira, 1990). The geological structure is folded and thrusted in a NW–SE direction and later cut by a series of NNE–SSW dextral strike-slip faults, events that took place during the different deformation phases of the Variscan orogenic cycle. The NW–SE striking lithologies have been offset by the left-handed strike-slip NW–SE Messejana Fault, a major structure that cuts across the crust and extends for hundreds of kilometers. The massive sulfide deposits are mainly composed of pyrite FeS_2, sphalerite (Zn,Fe)S, galena PbS, chalcopyrite $CuFeS_2$, and minor arsenopyrite FeAsS with average grades of 1% Cu, 3.5% Zn, 1.2% Pb, 1 ppm Au and 35 ppm Ag (Barriga and Fyfe, 1998). Some of these deposits occur at shallow levels and have been extensively oxidized forming a gossan with some Au concentrations that were exploited in Roman times.

3. Materials and methods

3.1. Sampling and samples preparation

Sampling included stream sediments and surface waters, and was performed along one of the streams draining the mining area of Aljustrel, Ribeira da Água Forte, and from both the major mine acid water dam where water and wastes from the mining processing plant are retained and from the tailings acid water pond (Fig. 2). Surface waters (sample reference AJTA) were collected in June–July 2006 and March 2007, using two 2-L polyethylene bottles for major ions. Water samples for major ion analysis were processed within 24 h. All bottles used for sampling were previously rinsed with a reagent grade acid solution and filled twice with the water to be sampled before its collection. Smaller 100 mL bottles were used to collect waters for trace metal analyses, which were subsequently acidified with 0.5 mL HNO_3 (p.a.). The analyses were performed at the Water Analysis Laboratory (Instituto Superior Técnico, Lisbon; all analytical procedures are certified by the norm NP EN ISO/IEC 17025) for the major ions. The analytical techniques included: Molecular Absorption Spectrophotometry (NH^{4+}, NO_2^-), Ion Chromatography (Cl^-, NO_3^{2-}, SO_4^{2-}), Flame Atomic Absorption Spectrometry (Ca^{2+}, Mg^{2+}), Flame Photometry (K^+, Na^+) and Thermal Atomization Atomic Absorption Spectrometry (Fe^{2+}).

Please cite this article in press as: Maia, F., et al. Metal partitioning in sediments and mineralogical controls on the acid mine drainage in Ribeira da Água Forte (Aljustrel, Iberian Pyrite Belt, Southern Portugal). Appl. Geochem. (2012), http://dx.doi.org/10.1016/j.apgeochem.2012.02.036

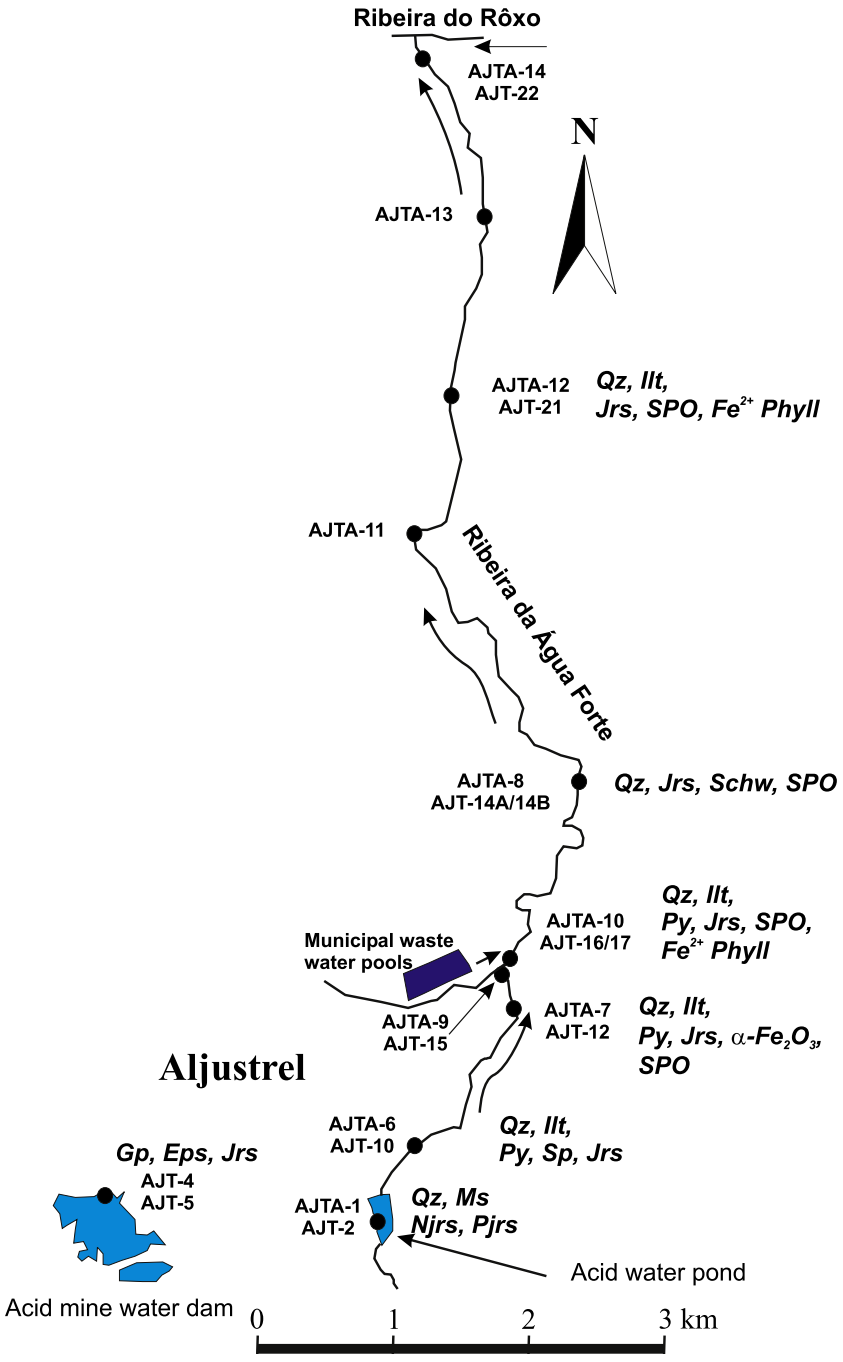

Fig. 2. Simplified map with the location of the sampling points for waters and sediments in the Ribeira da Água Forte. Also indicated are the location of the acid mine water dam (near the mining processing plant), the acid water pond (in the tailings area), the municipal waste water pools, and the flow path. The mineralogy identified by XRD and Mössbauer spectroscopy is indicated near the corresponding samples. Mineral abbreviations follow, whenever possible, the Whitney and Evans (2010) rules and listing updated from Kretz (1983): Qz – quatz; Ilt – illite; Ms – muscovite; Gs – gypsum; Eps – epsomite; Jrs – jarosite; Njrs – natrojarosite; Pjrs – plumbojarosite; Py – pyrite; Sp – sphalerite; Schw – schwertmannite; SPO – small particle Fe oxyhydroxides; Fe^{2+} Phyll – Fe^{2+} containing phyllosilicates. All water samples are referenced as AJTA, and all sediment samples are referenced as AJT.

Trace elements were analyzed at the Activation Laboratories (Canada; certification ISO/IEC 17025) with Inductively Coupled Plasma Mass Spectrometry (ICP-MS). Samples which were over the analytical range for specific elements were additionally analyzed by Inductive Coupled Plasma-Optical Emission Spectroscopy (ICP-OES). Electrical conductivity and temperature measurements were made using the WTW LF91 conductivity meter with a WTW KLE 1/T cell coupled with a calibrated temperature probe. Water pH and Eh were measured with a WTW pH323 pH meter using a WTW SenTix 50 Ag/AgCl electrode (pH), and an E56 Pt electrode with a reference Ag/AgCl electrode (redox). Speciation calculations and geochemical modeling were performed with PHREEQC using the phreeqc.dat database with no modifications (Parkhurst and Appelo, 1999).

The sediments were collected at the same sample sites as water whenever accessibility was possible and sufficient sediment was available for sampling (sample reference AJT). These sediments represent the solid phases that interact with the aqueous phase that percolated through the mine dumps. They include eight of the 10 sample sites for water, selected in order to characterize the AMD system at proximal and distal points. Surface sediment samples were collected and stored in plastic bags and polyethylene

Please cite this article in press as: Maia, F., et al. Metal partitioning in sediments and mineralogical controls on the acid mine drainage in Ribeira da Água Forte (Aljustrel, Iberian Pyrite Belt, Southern Portugal). Appl. Geochem. (2012), http://dx.doi.org/10.1016/j.apgeochem.2012.02.036

bottles. Sediment samples with references AJT-14A and AJT-14B were collected at the same spot and represent the surficial, up to 10 mm thick deposit of orange-red material (mostly Fe oxyhydroxides in a floccy material) and the underlying dark sediment, respectively. Samples AJT-16 and AJT-17 were both collected at the location where acid waters and organic-rich waste waters mix. Samples AJT-4, and AJT-5 are from the acid–water dam that collects the water and wastes from the mining processing plant and AJT-1 is from the tailings pond that feeds the Ribeira da Água Forte.

Sediment samples were oven dried at 30 °C for up to 48 h depending on humidity. They were subsequently disaggregated with a rubber-head hammer, homogenized, sieved (<90 μm), and then divided into 10 g portions. Samples for the sequential extraction procedures were dried at 105 °C overnight in order to release residual water. The chemical composition of these sediments was determined at the Activation Laboratories (Canada) by Instrumental Neutron Activation Analysis (INAA) and ICP-MS, using a four-acid (HF, $HClO_4$, HNO_3 and HCl) digestion technique.

3.2. Mössbauer spectroscopy and X-ray diffraction

A subset of the sediment samples was selected for Mössbauer spectroscopy, including sediments from low pH waters (≈2), from the mixing zone of acid waters with organic-rich waste waters, and further downstream. The ^{57}Fe Mössbauer measurements were recorded between 295 and 4.2 K in transmission mode using a conventional constant acceleration spectrometer and a 25-mCi ^{57}Co source in Rh matrix. The velocity scale was calibrated using an α-Fe foil at room temperature. Isomer shift values are given relative to this standard. Powdered samples were gently packed together with Lucite powder into Perspex holders, in order to obtain homogeneous and isotropic Mössbauer absorbers containing about 5 mg/cm^2 of natural Fe. Low-temperature measurements were performed using a bath cryostat with the sample immersed in liquid He for measurements at 4.2 K and in He exchange gas for temperatures >4.2 K. The spectra were fitted to Lorentzian lines using a non-linear least-squares method (Figueiras and Waerenborgh, 1997). Relative areas and line widths of both peaks in a quadrupole doublet and of peak pairs 1–6, 2–5 and 3–4 in a magnetic sextet were constrained to remain equal during the refinement procedure. Distributions of quadrupole or magnetic splittings were fitted according to the histogram method.

Powder X-ray diffraction (XRD) was performed with a Rigaku MiniFlex II diffractometer, using Cu Kα radiation with an output voltage of 30 kV and an output current of 15 mA, a graphite crystal monochromator, and a detector with a NaI(T1) scintillator and a Be window. Samples were scanned in the 3–90° range with steps of 0.02° in continuous mode, at a rate of 0.40°/min. The same powdered samples were also reacted with a mixture of oxalic acid and ammonium oxalate for 4 h in the dark to dissolve poorly crystalline Fe phases, and other metastable phases, and were reanalyzed by XRD.

Mineral identification was done with the aid of the software Identify (Carvalho, 1998), which assigns the diffraction peaks to the reported peaks in the Powder Diffraction File from the JCPDS-ICDD, ordering the minerals according to the number of peaks matched relative to the number of peaks present. The analysis of the diffractograms required careful post-processing to eliminate spurious matches of mineral peaks and reduce the number of workable hypotheses to a reasonable number of minerals to work with.

3.3. Sequential extraction

The sequential extraction procedure was performed in duplicate and the sequence was adapted to handle samples affected by AMD, because of their large Fe content and the presence of sulfides in some of them. A total of five sequential extraction schemes were attempted, but only the last two were successful and gave acceptable results. Due to the necessity of trying so many attempts, the stock of samples AJT-14A and AJT-14B ran out and it was necessary to collect more for the two last extraction schemes. The samples were collected at the same place, but two years after the first sampling; and because of the dynamic nature of this system, chemical differences are expected. Furthermore the underlying sediment (14B) was much more mixed with surface material than it was during the first sampling survey. In the selected extraction sequence, the organic matter step is performed according to Breward et al. (1996) and before the Fe–Mn oxyhydroxides step, and this last step is split into two substeps in order to enhance the recovery from the oxyhydroxide phases. The whole sequence is summarized in Table 1. For each extraction sequence, 2 g of sediment sample dried at 105 °C overnight was weighed. All experimental procedures used reagent grade solutions and doubly-distilled water. At the end of each extraction step or sub-step the volume of the extraction solution used in each sample is measured and the solution collected and stored in polyethylene bottles and stored in a freezer at <4 °C for later analysis. In addition, the solid residual phase from each extraction step or sub-step is washed with distilled water and centrifuged. The liquid fraction is discarded and the solid fraction dried at 105 °C for 24 h. The solid fraction is weighed after drying to be used in the subsequent step. The extraction steps comprised the following:

E1. Easily exchangeable (non-specific adsorbed): 16 mL of ammonium nitrate (1 M) are added to the sediment and shaken for 45 min in an orbital shaker. The solution is then centrifuged at 4000 rpm for 30 min.

E2. Specifically adsorbed: 16 mL of ammonium acetate (1 M) are added to the residue from the previous extraction, following the same procedures as previously described.

E3. Bound to organics: this third step is divided in two sub-steps (E3A and E3B). In sub-step E3A, 32 mL of NH_4OH (1 M) are added to the residue from the previous extraction and shaken for 2 h. Then, the mixture is centrifuged at 4000 rpm for 30 min. The volume of the supernatant is measured and acidified to pH = 1 with concentrated HCl (37 % v/v), and reserved for 24 h. If a precipitate forms, the solution is then centrifuged at 2000 rpm for 15 min and the precipitate is collected for step E3B. The supernatant volume is collected for analysis in polyethylene bottles. For sub-step E3B, a solution of 16 mL of H_2O_2 (30 % w/v) acidified to pH = 2 with HNO_3 is added to the precipitate and placed in a temperature controlled water bath at 85 ± 2 °C until it completely dissolves. The solution volume is collected for analysis in polyethylene bottles. The sediment residue of sub-step E3A follows the general procedure to be used in step E4.

E4. Bound to oxyhydroxides: the fourth extraction step is also split into two sub-steps (E4A and E4B). In sub-step E4A, 40 mL of sodium citrate (0.3 M) and 5 mL of sodium bicarbonate (0.5 M) are added to the residue and shaken for 10 min, after which 1 g of sodium dithionite is added and the solution is manually shaken for 1 min. The solution is transferred in a temperature controlled water bath where it is heated at 80 ± 2 °C for 15 min. The mixture is then centrifuged at 4000 rpm for 30 min. In sub-step E4B, 80 mL of Tamm's Reagent (a mixture of oxalic acid and ammonium oxalate) are added to the residue and shaken in the dark for over 4 h to attack poorly crystalline Fe oxyhydroxides. The remaining procedures are performed as previously described.

E5. Residual: for the final extraction, 1 g of the sediment residue from the last step is digested by dissolving it in a mixture of 15 mL HF and 15 mL $HClO_4$ at high temperature until the

Please cite this article in press as: Maia, F., et al. Metal partitioning in sediments and mineralogical controls on the acid mine drainage in Ribeira da Água Forte (Aljustrel, Iberian Pyrite Belt, Southern Portugal). Appl. Geochem. (2012), http://dx.doi.org/10.1016/j.apgeochem.2012.02.036

Table 1
Summary of sequential extraction steps and general procedures.

Extraction steps	Description			Reagents	Observations
E1	Easily exchangeable/non-specific absorbed			NH_3NO_3 (1 M)	Continuous agitation (45 min); room temperature
E2	Specific absorbed			NH_4OAc (1 M)	Continuous agitation (45 min); room temperature
E3	Bound to organic matter	A	Fulvic acid	NH_4OH (1 M); HCl (37% v/v)	Continuous agitation (2 h); room temperature
		B	Humic acid	HNO_3 (0.02 M) H_2O_2 (30%, pH 2 with HNO_3)	Some agitation (10 min at 85 ± 2 °C)
E4	Bound to iron oxyhydroxides	A	Fe-1	$C_6H_9Na_3O_9$ (0.3 M); $NaHCO_3$ (0.5 M) $Na_2S_2O_4$	Continuous agitation (10 min + 1 min) Some agitation (15 min at 80 ± 2 °C)
		B	Fe-2	Tamm reagent	
E5	Residue			HF; $HClO_4$; HCl (37% v/v)	

solution evaporates completely. This procedure is repeated three times. Afterwards, an additional 15 mL of $HClO_4$ are added to the residue and heated until it fully evaporates. Finally, a volume of 20 mL of concentrated HCl (37 % v/v) is added to dissolve the residue which is then diluted with doubly distilled water and brought to a volume of 100 mL.

Analyses of the metal content (Cu, Zn, and Pb) in the solutions obtained from the sequential extraction were carried out by Flame Atomic Absorption Spectrophotometry (AAS) with a Varian SPECTRAA FS 220. A calibration curve was constructed in each analytical session with in-house standard solutions. Solutions with Tamm's reagent were previously subjected to an acid attack with aqua regia at high temperature to decompose oxalate, removing the undesirable signal depression from the metals in the analysis with AAS caused by the oxalate complex.

4. Results and discussion

Surface waters flowing along the Ribeira da Água Forte result mainly from the interaction with the mine waste pile that existed in the town of Aljustrel. Presently, only patches of the original pile exist on-site since the site has long been reclaimed, but the mining operation still continues to this day and the site remains partially flooded forming a pond of acid water. The piles of waste rock (mostly the sulfide mineralization host rocks) still remaining on site continue to interact with surface waters, mainly from rainfall but also from the site operation; even the minor disseminated sulfide in the waste rocks is sufficient to keep feeding acid waters to the watershed. These waters flow northwards for approximately 10 km until they join the waters from the E–W Ribeira do Rôxo (Fig. 2). However, approximately 2 km from the source area of the waste-rock piles the Ribeira da Água Forte receives a continuous input of municipal waste waters from the town of Aljustrel. These waters result from the overflow of two collecting pools several meters above the stream bed, which discharge into the Ribeira da Água Forte without treatment. Therefore, these organic-rich, high pH, waters have the effect of neutralizing the acid-mine waters that they encounter. The effects are immediately visible because the stream banks of the Ribeira da Água Forte upstream are barren and devoid of any plants or grass, a situation that changes completely just after the mixing zone. Additionally, the flow conditions are markedly different during the summer and the winter. Summer conditions, due to low precipitation, are characterized by very low water fluxes or even a dry stream bed between the mine waste-rock piles and the mixing zone. In such a situation, the overflowing organic-rich waste waters are the only source of waters for the Ribeira da Água Forte from that point onwards. Under wetter conditions, the water flux coming from the mine waste-rock site is continuous along the Ribeira da Água Forte, but oscillates in response to rainfall. These particular conditions gave rise to a distinct pattern on the measured parameters and dissolved ions before and after the water mixing zone (Table 2; Fig. 3).

In the description that follows, results will be presented referring to the different segments of the Ribeira da Água Forte, namely from the source until the mixing with the waste waters (i.e., a "typical" AMD system), in the mixing zone, and from that point downstream.

4.1. Mineralogy and geochemistry of the AMD system

The waters upstream of the mixing zone show that changes in the elemental concentrations in summer or winter result from concentration/dilution effects due to drier or wetter weather, respectively. This is particularly evident in the conductivity measurements (Fig. 3A). These effects also induce changes on the measured pH that rise from values just below 2 to around 2.5 on average (Fig. 3B). Furthermore, elemental concentrations in the sampled waters are within the same order of magnitude as in the source acid pond that feeds the stream. Apart from the very high SO_4^{2-} and Fe content of the waters, most of which is in colloidal form in the very acid waters, the transition metals and other trace elements, derived from the sulfide-rich rocks in the waste piles have very significant concentrations. Copper and Zn are the most abundant followed by Co, Cd, As, Ni, and Pb (Fig. 3C–H; Table 2).

Trace element concentrations in sediments (Fig. 4 and Table 3) are equally high, typically above 1000 ppm for Cu, Zn, As and Ba, but Pb has values in excess of 5000 ppm. In contrast, Co, Cd, and Ni have concentrations up to tens of ppm if not less. The discrepancy between the magnitude of the concentration of metals such as Pb, Ni, Co, Cd and Ba in the sediments compared to those in the waters collected at the same sites is notable (Tables 2 and 3). This difference immediately highlights the relative importance of partitioning and uptake of these metals by the sediments, either by mineral precipitation or by adsorption.

Stream sediments were sampled during the drier season when the stream bed in this branch was commonly dry with scattered small pools of stagnant acidic waters. The stream bed is also normally rocky and devoid of significant sediment accumulation but the sediments patches occurring upstream towards the mine-waste piles, which are the source of the AMD, are often above the water level. The repeated sub-aerial exposure of these sediments and the high SO_4^{2-} concentrations of the waters are reflected in the abundance of gypsum and jarosite group minerals in the sediments. Also, minor quantities of pyrite and sphalerite have been detected by XRD. Jarosite-group minerals that occur in the sediments from the acid pond were identified by XRD as being mostly natrojarosite $\left(NaFe_3^{3+}(SO_4)_2(OH)_6\right)$ with the possible presence of plumbojarosite $\left(PbFe_6^{3+}(SO_4)_4(OH)_{12}\right)$. Samples AJT-4 and AJT-5 (from the acid-mine water dam) have mostly precipitates from mine-water discharges, which are composed of gypsum

Please cite this article in press as: Maia, F., et al. Metal partitioning in sediments and mineralogical controls on the acid mine drainage in Ribeira da Água Forte (Aljustrel, Iberian Pyrite Belt, Southern Portugal). Appl. Geochem. (2012), http://dx.doi.org/10.1016/j.apgeochem.2012.02.036

Table 2
Composition of water samples along the Ribeira da Água Forte. Samples are ordered by increasing distance from the source of the acid waters in the tailings area. Waters collected in each sampling campaign were assigned an extra label, 1 for the summer (June/July 2006), and 2 for winter (March 2007). The references for the sediments collected at the same spots are indicated as well. Sample AJTA-1 was collected only in the summer; resuming of mining operations impeded the access to the spot in the winter. The gray strip on the table corresponds to the samples taken at the mixing zone. Sulfate concentration reported for sample AJTA-11-2 is most probably due to an unidentified laboratory error.

Sediments	Water samples	Dist. (km)	pH	Cond. (mS/cm)	NH^{4+} (mg/L)	Ca^{2+} (mg/L)	Fe^{2+} (mg/L)	Mg^{2+} (mg/L)	K^{+} (mg/L)	Na^{+} (mg/L)	HCO_3^- (mg/L)	Cl^- (mg/L)	NO_3^{2-} (mg/L)	NO_2^- (mg/L)	SO_4^{2-} (mg/L)
AJT-2	AJTA-1-1	0													
AJT-10	AJTA-6-1	0.44	2.0	14.8	0.7	389	4800	973	2	24		126	12	0.3	33,000
AJT-12	AJTA-7-1	1.82	2.0	13.8	0.7	388	4900	831	2	42		160	12	0.3	31,000
AJT-15	AJTA-9-1	2.12	2.0	13.7	0.9	350	4900	802	2	44		162	12	0.3	31,000
AJT-17	AJTA-10-1	2.24	8.4	2.3	49	79	0.49	52	21	240	439	429	0.3	0.3	137
AJT-14	AJTA-8-1	4.26	4.0	4.0	52	112	170	104	22	211		381	1.0	0.01	1900
	AJTA-11-1	6.82	3.9	3.4	49	111	55	86	22	243		437	0.6	0.01	1100
AJT-21	AJTA-12-1	8.02	3.9	3.8	49	138	40	87	20	242		446	1.0	0.01	1200
	AJTA-13-1	9.38	4.0	3.9	41	203	43	96	19	226		420	1.0	0.01	1500
AJT-22	AJTA-14-1	10.69	4.1	3.6	31	230	14	83	16	229		443	1.0	0.01	1300

	Water samples	Dist. (km)	Cu (μg/L)	Zn (μg/L)	Pb (μg/L)	Co (μg/L)	Ni (μg/L)	As (μg/L)	Cd (μg/L)	Ba (μg/L)
AJT-2	AJTA-1-1	0	362,000	574,000	34.1	6330	1940	1770	1330	
AJT-10	AJTA-6-1	0.44	432,000	711,000	72.7	7350	2400	9730	1640	5.0
AJT-12	AJTA-7-1	1.82	422,000	721,000	19.7	7190	2170	27,500	1560	1.0
AJT-15	AJTA-9-1	2.12	397,000	678,000	34.7	6690	2020	29,000	1480	1.0
AJT-17	AJTA-10-1	2.24	166	720	4.6	5.1	31	12.80	1.4	52.0
AJT-14	AJTA-8-1	4.26	14,900	37,300	520	384	212	79.50	70.1	51.2
	AJTA-11-1	6.82	3710	16,700	25.0	160	140	8.89	25.5	19.1
AJT-21	AJTA-12-1	8.02	3620	16,600	23.3	153	176	5.99	26.4	13.5
	AJTA-13-1	9.38	6660	28,800	27.5	291	211	10.50	52.1	16.9
AJT-22	AJTA-14-1	10.69	3630	17,700	10.6	144	167	5.80	40.4	12.2

	Water samples	Dist. (km)	pH	Cond. (mS/cm)	NH^{4+} (mg/L)	Ca^{2+} (mg/L)	Fe^{2+} (mg/L)	Mg^{2+} (mg/L)	K^{+} (mg/L)	Na^{+} (mg/L)	HCO_3^- (mg/L)	Cl^- (mg/L)	NO_3^{2-} (mg/L)	NO_2^- (mg/L)	SO_4^{2-} (mg/L)
AJT-10	AJTA-6-2	0.44	2.4	11.0		241	3900	394	5.9	38		83			16,000
AJT-12	AJTA-7-2	1.82	2.6	7.9		227	2100	356	10	48		83	14		12,000
AJT-15	AJTA-9-2	2.12	2.6	7.0	12	241	1800	280	10	48		75	53		10,000
AJT-17	AJTA-10-2	2.24	4.8	3.4	35	100	280	90	17	137		221	13		1900
AJT-14	AJTA-8-2	4.26	4.9	3.1		76	210	71	12	121		206	3		1500
	AJTA-11-2	6.82	4.7	3.5		93	250	87	11	118		202	5		2
AJT-21	AJTA-12-2	8.02	4.2	3.3		106	180	83	9.5	120		217	5		1600
	AJTA-13-2	9.38	4.7	3.9		128	160	80	9.4	121		219	6		1600
AJT-22	AJTA 14	10.69	4.5	3.1		120	120	77	8.6	124		229	6		1500

	Water samples	Dist. (km)	Cu (μg/L)	Zn (μg/L)	Pb (μg/L)	Co (μg/L)	Ni (μg/L)	As (μg/L)	Cd (μg/L)	Ba (μg/L)
AJT-10	AJTA-6-2	0.44	206,000	452,000	122	3670	1110	12,800	987	10
AJT-12	AJTA-7-2	1.82	130,000	355,000	4.0	2910	1350	5820	784	10
AJT-15	AJTA-9-2	2.12	110,000	308,000	109	2610	1160	5320	695	10
AJT-17	AJTA-10-2	2.24	22,900	64,200	24.1	521	276	871	139	30
AJT-14	AJTA-8-2	4.26	15,500	42,800	25.3	535	159	210	87.3	21
	AJTA-11-2	6.82	20,800	60,700	27.0	489	213	120	128	23
AJT-21	AJTA-12-2	8.02	17,700	50,200	22.7	404	195	41.6	103	20
	AJTA-13-2	9.38	15,200	45,400	20.2	385	188	30.1	101	20
AJT-22	AJTA-14-2	10.69	14,100	41,800	17.8	332	167	18.2	85.9	15

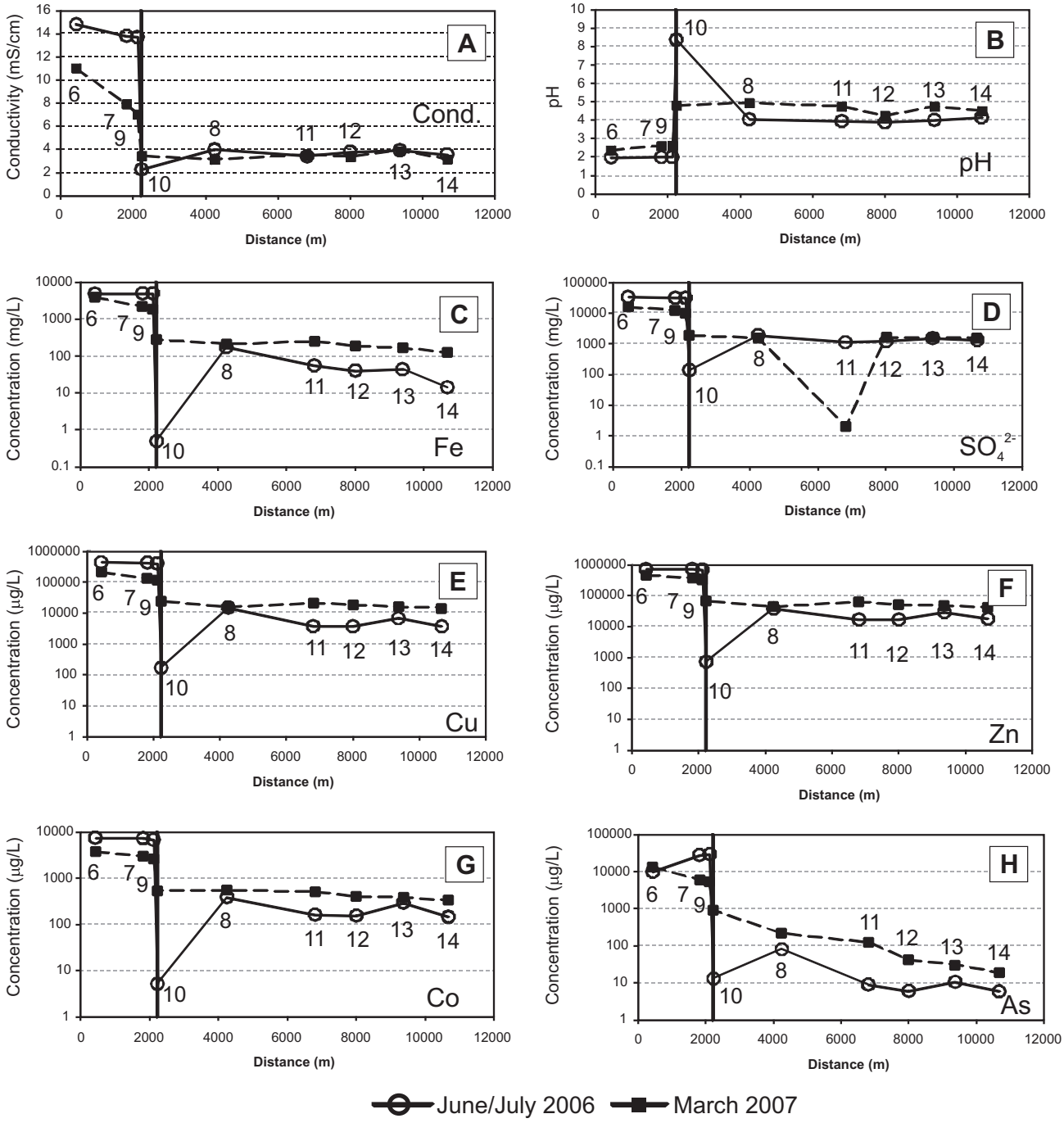

Fig. 3. Trace element and anion concentration and parameter profiles of water samples as a function of distance along the Ribeira da Água Forte. Labeled numbers of the samples (AJTA) are indicated near each plotted point. Distance is measured from the acid water pond in the tailings area in the Aljustrel village, and the vertical black line marks the position of the mixing zone. The anomalously low SO_4^{2-} concentration reported is probably due to an analytical error.

($CaSO_4{\cdot}2H_2O$) and epsomite ($MgSO_4{\cdot}7H_2O$) (Fig. 5). The treatment of these samples with the mixture of ammonium oxalate with oxalic acid completely dissolved these minerals and promoted the precipitation of the oxalate crystals whewellite (composed of $Ca(C_2O_4){\cdot}H_2O$) and glushinskite ($Mg(C_2O_4){\cdot}H_2O$). The mineralogy of the clastic stream sediments (including the sediments from the acid pond) reflects the nature of the basement rocks of the Aljustrel volcanic complex, where quartz, muscovite and/or illite are ubiquitous.

Along this branch of the Ribeira da Água Forte, only sample AJT-12 was analyzed by Mössbauer spectroscopy. However, due to the presence of a large number of Fe-bearing phases in all the samples analyzed, some of which have similar hyperfine parameters, spectra were taken at different temperatures between 295 and 4 K in order to distinguish some of these phases from one another. Therefore, the analyses of the AJT-12 spectra will be discussed in detail. A similar reasoning was followed for the remaining samples that are discussed below. The main features of the room temperature Mössbauer spectrum of AJT-12 (Fig. 6) are two quadrupole doublets with isomer shifts (IS) at 0.34 and 0.39 mm/s and quadrupole splittings (QSs) at 0.64 and 1.23 mm/s (Table 4). The doublet with lower IS and QS is similar to those commonly observed in sediments or soil samples, due to both Fe^{3+} in phyllosilicates and small particle Fe^{3+} oxides-oxyhydroxides (SPOs) with a superparamagnetic

Please cite this article in press as: Maia, F., et al. Metal partitioning in sediments and mineralogical controls on the acid mine drainage in Ribeira da Água Forte (Aljustrel, Iberian Pyrite Belt, Southern Portugal). Appl. Geochem. (2012), http://dx.doi.org/10.1016/j.apgeochem.2012.02.036

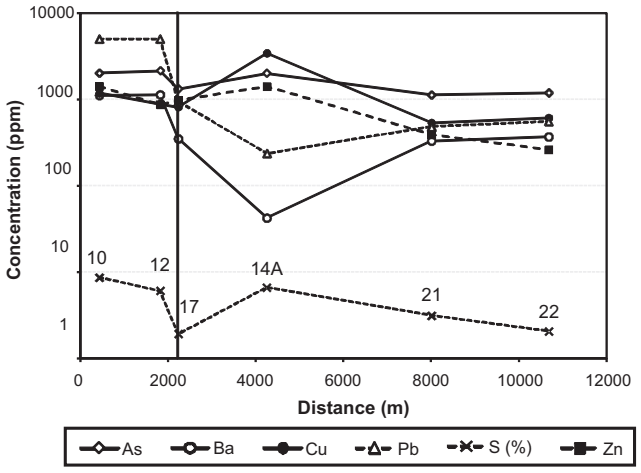

Fig. 4. Concentration profiles for some trace elements and S in sediments along the Ribeira da Água Forte, as a function of distance. Labeled numbers of the samples (AJT) are indicated near each plotted point. The vertical black line marks the position of the water mixing zone. Element concentration is in ppm except for S (in %), as indicated.

behavior at room temperature and blocking temperatures in the range 295–4 K (Coey, 1988; Murad, 1988, 1998; Vandenberghe et al., 2000). SPO that occur in weathering environments may include microcrystalline hematite, hydroxyl-containing hematite and goethite with different particle sizes where Fe^{3+} may be, in part, substituted by other cations, commonly Al^{3+}, and ferrihydrite ($Fe_5HO_8{\cdot}4H_2O$), the poorly ordered hydrous Fe oxide generally formed by the rapid oxidation of Fe-bearing solutions (Murad, 1988, 1998). Pyrite is not only expected to be present but has also been identified by XRD. Because it will contribute to the doublet with lower IS and QS, low-temperature spectra are necessary to reach a definitive answer. The parameters of the doublet with higher IS and QS are similar to those reported for jarosite (Murad, 1998). In particular, QS = 1.23 mm/s is characteristic of this hydroxysulfate and significantly higher than the QS values of superparamagnetic SPO (Murad, 1988, 1998). In the 295 K spectrum a small peak is observed at approximately 2.35 mm/s suggesting a third quadrupole doublet with much higher IS and QS typical of Fe^{2+} in phyllosilicates (McCammon, 1995; Murad, 1998). Finally small peaks at velocities higher than 4 mm/s and lower than −4 mm/s were also detected. They indicate the presence of a sextet with estimated parameters

Table 3
Stream sediment composition of major elements and selected trace elements. As in Table 2, samples are ordered by increasing distance from the source, and references for water samples collected at the same spots are also indicated. The gray strip on the table corresponds to samples taken at the mixing zone.

Water	Sediment sample	Dist. (km)	SiO_2 (%)	Al_2O_3 (%)	Fe_2O_3 (%)	MnO (%)	MgO (%)	CaO (%)	Na_2O (%)	K_2O (%)	TiO_2 (%)	P_2O_5 (%)	LOI (%)
AJTA-6	AJT-10	0.44	34.61	11.74	17.24	0.02	0.55	0.15	0.91	2.4	0.35	0.12	25.80
AJTA-7	AJT-12	1.82	46.24	13.72	12.85	0.01	0.56	0.14	1.20	2.53	0.53	0.13	18.30
AJTA-10	AJT-17	2.24	53.64	8.44	13.73	0.04	0.81	0.75	1.11	1.23	0.59	0.72	17.51
AJTA-8	AJT-14A	4.26	0.70	0.87	52.81	0.04	0.43	0.25	0.55	0.55	0.01	0.39	42.02
AJTA-8	AJT-14B	4.26	25.56	11.24	32.27	0.07	0.69	0.56	0.66	1.53	0.39	1.00	25.13
AJTA-12	AJT-21	8.02	31.39	9.89	30.80	0.03	0.74	0.29	0.96	2.09	0.52	0.35	23.60
AJTA-14	AJT-22	10.69	41.53	9.07	27.78	0.05	0.63	0.27	0.77	1.67	0.72	0.27	16.75

		Dist. (km)	As (ppm)	Ba (ppm)	Cd (ppm)	Co (ppm)	Cr (ppm)	Cu (ppm)	Ni (ppm)	Pb (ppm)	S (%)	Zn (ppm)
AJTA-6	AJT-10	0.44	2020	1110	4.5	20	26	1180	9	>5000	8.63	1410
AJTA-7	AJT-12	1.82	2140	1130	2.7	14	32	883	14	>5000	6.03	868
AJTA-10	AJT-17	2.24	1320	349	2.9	9	47	812	22	938	1.9	981
AJTA-8	AJT-14A	4.26	2000	42	3.0	14	15	3420	8	235	6.62	1400
AJTA-8	AJT-14B	4.26	2880	330	4.7	16	54	1370	29	542	2.79	1530
AJTA-12	AJT-21	8.02	1130	329	0.8	7	46	533	23	479	3.12	387
AJTA-14	AJT-22	10.69	1190	367	<0.5	9	76	608	25	555	2.06	260

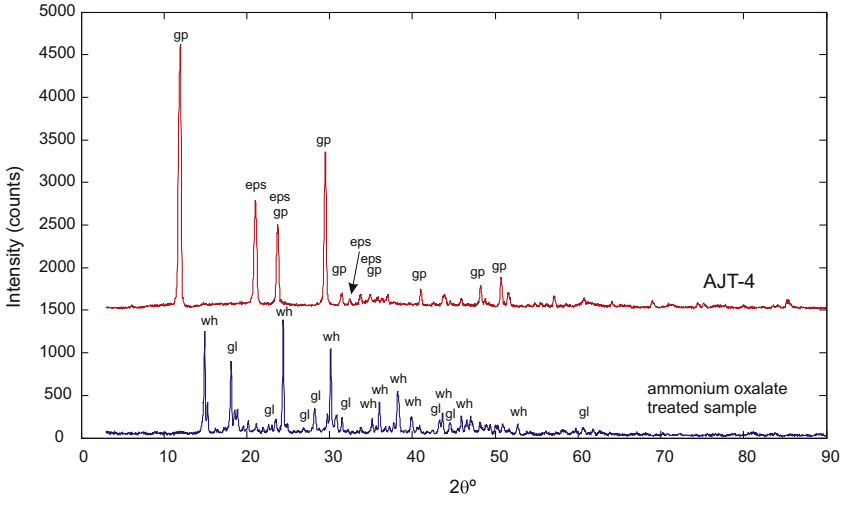

Fig. 5. X-ray diffractogram (Cu Kα) of sample AJT-4; ammonium oxalate treated sample below, and untreated sample above shifted 1500 units. Minerals in sample AJT-4, gypsum (gp) and epsomite (eps), were fully dissolved and precipitated as new oxalate phases, whewellite (wh) and glushinskite (gl).

Please cite this article in press as: Maia, F., et al. Metal partitioning in sediments and mineralogical controls on the acid mine drainage in Ribeira da Água Forte (Aljustrel, Iberian Pyrite Belt, Southern Portugal). Appl. Geochem. (2012), http://dx.doi.org/10.1016/j.apgeochem.2012.02.036

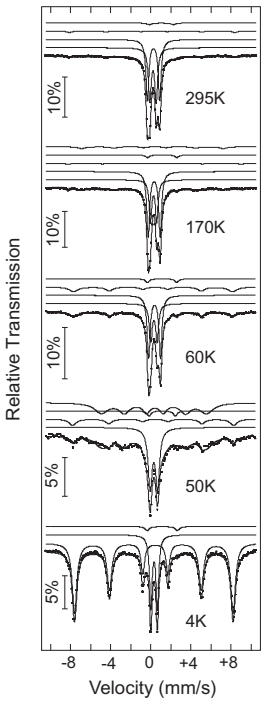

Fig. 6. Mössbauer spectra of AJT-12 sediment sample taken at different temperatures. The lines over the experimental points are the sum of sextets or doublets, shown slightly shifted for clarity, corresponding to Fe atoms on different phases (see text and Table 4).

similar to those of bulk hematite (Abreu et al., 1988; Murad, 1988; Vandenberghe et al., 2000).

At 170 and 60 K, spectral contributions from jarosite, Fe^{2+} in phyllosilicates and bulk hematite are present with the same relative areas as at 295 K, confirming the reliability of the analyses performed for this segment of spectra. The relative area, *I*, of the doublet with IS = 0.39 mm/s and QS approximately 0.63 mm/s decreases and a sextet with average magnetic hyperfine field $B_{hf} \sim 43.5$ T (170 K), 48.7 T (60 K) appears. The *I* value of this sextet increases with decreasing temperature and within experimental error is equal to the decrease in *I* of the QS ~ 0.63 mm/s doublet. This confirms that at least part of the Fe contributing to this doublet is due to SPO. The smaller SPO particles sizes correspond to lower blocking temperatures, i.e., the temperature at which their magnetic moments freeze relative to the Mössbauer effect observation time window giving rise to magnetic sextets in the spectrum. The spread in freezing temperatures may also be due to variation in local chemical composition arising from different degrees of substitution of Fe^{3+} by a multitude of impurity elements.

At 50 K, whereas the doublet with smaller QS ~ 0.63 mm/s is still present, it is clear that the doublet with QS ~ 1.2 mm/s disappears and a sextet with very broad peaks appears instead. This confirms the assignment of the QS ~ 1.2 mm/s doublet to jarosite. The reported magnetic ordering temperatures, the Neel temperature (T_N), of this hydroxysulfate are within the range 54–60 K (Murad, 1998; Bigham and Nordstrom, 2000). Therefore, the doublet observed in the paramagnetic state vanishes below 60 K, giving rise to a magnetic sextet. The fact that jarosite may have impurity cations replacing Fe^{3+} and defects in the crystalline structure, is reflected in slightly different relaxation times of the Fe^{3+} magnetic moments close to the T_N, which explain the broad magnetic peaks observed for the corresponding sextet, which are difficult to resolve from those of the other sextets due to SPO.

Finally at 4 K all the Fe^{3+} magnetic moments in jarosite are set. The same happens for practically all Fe^{3+} magnetic moments in SPO (Murad, 1998). This is consistent with the magnetic sextet peaks being significantly sharper than at 50 K. Because the magnetic hyperfine field, B_{hf}, of jarosite at 4 K (~47–48 T) is close to those of most SPO (Murad, 1998; Bigham and Nordstrom, 2000; Vandenberghe et al., 2000) the contributions of these phases are not resolved. The doublet with QS = 0.64 mm/s is clearly observed and has a reasonably high *I* (~22%). As referenced above, most SPO particles should have their magnetic moments set at 4 K giving rise to a magnetic sextet in the spectrum. It is also unlikely that such a high fraction of the total Fe (~22%) is due to paramagnetic Fe^{3+} incorporated in phyllosilicates, because Fe^{3+} is not a major constituent of these phases and the amount of phyllosilicates detected by XRD is vanishingly small. Considering further that QS = 0.64 mm/s and IS = 0.43 mm/s at 4 K are within experimental error the values reported for pyrite (Finklea et al., 1976; Cheetam et al., 1981), it is reasonable to assume that the corresponding doublet observed at 4 K is essentially only due to Fe in this sulfide.

The sequential extraction results for the set of samples in this branch of the Ribeira da Água Forte show that adsorption is the main scavenging mechanism for Zn (Table 5 and Fig. 7). Typically, non-specific adsorption (or easily exchangeable) of Zn is higher in the sediments of this branch, where it can account for up to 70% of the Zn in the sediment. Copper is also highly variable and non-specific adsorption generally contributes between 20% and 30% of this element in the sediment. Lead, in turn, is basically absent as an adsorbed phase, which is not surprising because of the highly discrepant values of Pb in the sediments and in the waters. Other major phases to which metals are associated include Fe oxyhydroxide and residual phases. Lead is mostly extracted (>80%) in the last sequential extraction step, whereas the amount of Cu recovered in this step is between 50% and 70%. All three elements were extracted from the Fe oxyhydroxide phases in quantities ranging from 10% to 20%. However, the extreme richness in Fe oxyhydroxide phases of these sediments restricts the extraction efficiency achieved in these steps (Maia, 2010), so most probably an uncertain amount of these metals released in the last step may have been originally associated with the Fe oxyhydroxides, and this observation is equally valid for the remaining samples along the Ribeira da Água Forte that will be considered next.

4.2. Mineralogy and geochemistry of the mixing zone

In this zone, the Ribeira da Água Forte receives input from untreated municipal waste water throughout the year. This constant input maintains flow in the stream from this point downstream during the dry season. This water was analyzed during the dry season at the discharge point in the stream bed (AJTA-10-1). Chemically, the municipal waste water is low in all constituents in comparison to the AMD waters (Table 2; Fig. 3), with the exception of NH_3, K, Na and Cl. The measured pH is 8.4 in striking contrast with the values around 2 for the waters upstream, and the same is verified for conductivity. The streambed sediments in this zone are black in color, in part due to the presence of organic matter. As noted before, this zone is also characterized by the presence of flourishing grassland near the margins and on the stream banks.

In the wet season the mixture of waters leads to less dramatic changes in the profile of elemental concentrations along the stream. Most of these changes may be related to dilution effects because, as noted before, the waste water has very low concentrations of all of the main metals that characterize the AMD. The pH rises to 4.8 and the conductivity decreases to 3.4 mS/cm. In relation to the metals (Table 2), their concentrations decrease on average by an order of magnitude. To further unravel the reason for this decrease, the trends in the major anions and cations in the stream path in both seasons should be considered (Table 2), where some show conservative behavior. Among these, Cl is conservative, but also Na and

Please cite this article in press as: Maia, F., et al. Metal partitioning in sediments and mineralogical controls on the acid mine drainage in Ribeira da Água Forte (Aljustrel, Iberian Pyrite Belt, Southern Portugal). Appl. Geochem. (2012), http://dx.doi.org/10.1016/j.apgeochem.2012.02.036

Table 4
Estimated parameters from the Mössbauer spectra of the Ribeira de Água Forte sediment samples taken at different temperatures *T*.

Sample	*T*(K)	IS (mm/s)	QS or ε (mm/s)	B_{hf} (tesla)	*I* (%)	Fe species
AJT-12	295	0.34	0.64	–	43	Py + SPO
		0.39	1.23	–	51	Jrs
		1.17	2.39	–	3	Fe^{2+} phyllosilicate
		0.34	−0.18	51.2	3	α Fe_2O_3
	170	0.40	0.63	–	30	Py + SPO
		0.45	1.19	–	52	Jrs
		1.23	2.93	–	3	Fe^{2+} phyllosilicate
		0.38	−0.14	43.5	12	SPO
		0.38	0.27	53.6	3	α Fe_2O_3
	60	0.43	0.63	–	27	Py + SPO
		0.48	1.19	–	49	Jrs
		1.25	2.93	–	4	Fe^{2+} phyllosilicate
		0.47	−0.21	48.7	17	SPO
		0.46	0.32	54.1	3	α Fe_2O_3
	4	0.42	0.64	–	22	Py
		0.5	−0.16	49.4	76	Jrs + SPO + α Fe_2O_3
		1.26	2.86	–	2	Fe^{2+} phyllosilicate
AJT-16	295	0.34	0.62	–	60	Py + SPO + Schw?
		0.38	1.2	–	32	Jrs
		1.16	2.57	–	7	Fe^{2+} phyllosilicate
	4	0.42	0.66	–	31	Py
		0.5	−0.14	48.5	60	Jrs + SPO + Schw?
		1.27	2.91	–	9	Fe^{2+} phyllosilicate
AJT-14A	295	0.37	0.68	–	81	SPO + Schw?
		0.38	1.21		19	Jrs
Surface layer	4	0.49	−0.19	45.3	63	SPO + Schw?
		0.5	−0.09	49.4	21	SPO
		0.49	−0.22	47.3	16	Jrs
AJT-14-B	295	0.37	0.69	–	73	SPO + Schw?
		0.36	−0.11	25.3	22	SPO
		1.02	2.51	–	5	Fe^{2+} phyllosilicate
	4	0.48	1.05	–	4	Fe^{3+} phyllosilicate
		0.48	−0.18	48.7	93	SPO + Schw?
		1.21	2.85	–	3	Fe^{2+} phyllosilicate
AJT-21	295	0.38	0.55	–	61	SPO + Fe^{3+} phyllosilicate
		0.38	1.18	–	37	Jrs
		1.2	2.55	–	2	Fe^{2+} phyllosilicate
	4	0.48	0.73	–	4	Fe^{3+} phyllosilicate
		0.49	−0.22	50.0	95	SPO + Jrs
		1.28	3.02	–	2	Fe^{2+} phyllosilicate

IS isomer shift relative to metallic α-Fe at 295 K; QS and ε quadrupole splitting and quadrupole shift estimated for the doublets and sextets, respectively. B_{hf} magnetic hyperfine field; *I* relative area. Estimated errors $\leqslant$0.02 mm/s for IS, QS, <0.2 T for B_{hf} and <2% for *I*. Fe species: Py pyrite, Jrs jarosite, Schw? schwertmannite (unsure), SPO Fe^{3+} in small particle size oxides-oxyhydroxides, α Fe_2O_3 bulk hematite.

K display the same behavior. These elements may be used to quantify the relative amount of mixing between the waters (acid drainage water and waste water). A major drawback is that the waste water has only been properly analyzed in the dry season (AJTA-10-1); nevertheless both sources of waters, the feeding acid water pond and the municipal waste water pools, occupy similar areas and thus a reasonable approach could be to consider that the dilution factor for the waste water in the wet season is similar to the dilution factor estimated for the acid-drain waters in the same season. Thus, using Cl as reference, the acid water from the wet season shows a 0.4 dilution factor relative to the same water collected in the dry season, and applying this same factor to the concentrations in AJTA-10-1, the water at the mixing zone in the wet season could be the result of a mixture of 80% waste water and 20% acid water. This almost balances the resulting concentration in Cl in the mixed water sample (AJTA-10-2) but overestimates the Na concentration by about 9%. However, it matches quite remarkably the concentrations in Cu, Zn, Pb, Co and Cd with deviations of 3.5% for Cu and Zn, and less than 1% for the remaining metals. For Ni, the deviation deficit is 18%. For Fe and As, the concentrations are overestimated by 29% and 143%, respectively. The reason for these results will be later discussed while presenting a synthesis of the geochemical system of the Ribeira da Água Forte (Section 4.4).

The sediment collected and analyzed at this site (AJT-17) has similar concentrations of major elements as other samples, which reflects the nature of the bedrock. However, it shows a general decrease in most trace metals, but not as pronounced (Table 3; Fig. 4). As discussed above this stream has drained acid-mine waters for decades, and only more recently has it received this waste water input. Therefore, the stream sediments are likely to result from the inherited characteristics of acid drainage sediments, thus reinforcing the smaller differences observed. Also, the results of sequential extraction were not significantly different (Table 5 and Fig. 7). In spite of a greater input of organic matter in this zone from the waste water, only Cu was significantly extracted in the corresponding extraction step.

The mineralogy is also not significantly different from that previously observed, but the presence of distinctive peaks of pyrite in the XRD traces is worthy of note. The analysis of the 295 K and 4 K Mössbauer spectra of AJT-16 (Figs. 8 and 9) shows that in this sample pyrite and jarosite are present although the fraction of Fe in the hydroxysulfate is lower than in AJT-12 (Table 4). No bulk hematite is detected and most of the Fe is present as Fe^{3+} in SPO. The broad peaks of the sextet observed in the 4 K spectrum, which could only be fitted with a distribution of B_{hf}, result from the unresolved but slightly different contributions of this Fe^{3+} in SPO.

Please cite this article in press as: Maia, F., et al. Metal partitioning in sediments and mineralogical controls on the acid mine drainage in Ribeira da Água Forte (Aljustrel, Iberian Pyrite Belt, Southern Portugal). Appl. Geochem. (2012), http://dx.doi.org/10.1016/j.apgeochem.2012.02.036

Table 5
Analytical results of the solutions from each sequential extraction step (see Table 1), for Zn, Cu, and Pb. Concentrations are in ppm. Uncertainty in the total concentrations is typically between 10% and 20%. Extraction sequence was repeated twice for each sample (explanation in methods section) and the final column shows the relative difference between the totals from each of these extraction sequences. Blank cells mean that in the corresponding solutions the metal concentrations are below detection limits.

Sample	Extractions								Extractions								
	E1	E2	E3a	E3b	E4a	E4b	E5	Total	E1	E2	E3a	E3b	E4a	E4b	E5	Total	Diff. %
Zn																	
AJT-2	743	17	2	2	72	46	76	958	744	58		1	85	44	166	1098	12.8
AJT-10	695	27	3	2	96	81	94	998	719	48	5	3	197	31	851	1854	46.2
AJT-12	130	5	2	6	83	39	934	1199	129	5	4	1	79		885	1103	8.0
AJT-15	788	58	7	3	138	95	802	1891	719	16	4		122	61	820	1742	7.9
AJT-17	612	65	5	6	129	197	206	1220	516	39	5	2			190	752	38.4
AJT-14A	34	172	41	4	505	2656	1784	5196	27	68		4	2027	727	2277	5130	1.3
AJT-14B	173	165	34	3	224	1388	1003	2990	95		28	2	1085	702	976	2888	3.4
AJT-21	206	1	3	2	114	183		509	346	1	6	1	78	58		490	3.7
AJT-22	69	1	4	6		50	165	295	45		10	1	88	49	162	355	16.9
Cu																	
AJT-2	114	2	6	2	2	93	467	686	121	4	7	2	1	130	456	721	4.9
AJT-10	316	4	15	5	8	214	654	1216	317	8	23	17	1	331	664	1361	10.7
AJT-12	125	6	24	6	5	138	527	831	115	4	19	5	1	154	526	824	0.8
AJT-15	369	10	18	3	1	234	591	1226	379	5	13	2	1	262	558	1220	0.5
AJT-17	174	21	46	10	58	166	370	845	174	14	30	4	80	213	340	855	1.2
AJT-14A	2	46	104	15	87	614	982	1850	16	20	135	10	382	447	661	1671	9.7
AJT-14B	1	18	74	23	16	391	63	586	1	3	76	8	50	479	1246	1863	68.5
AJT-21	19	1	11	3	100	208	263	605	16	1	8	4	154	112	290	585	3.3
AJT-22	27	2	8	4	91	128	142	402	27	1	7	4	90	117	167	413	2.7
Pb																	
AJT-2	10	9		3	13	1067	7467	8569	5	8	1	131	144	1358	7489	9136	6.2
AJT-10	3	2	7	2	68	1271	10,997	12,350	3	2	12	21	234	858	11,488	12,618	2.1
AJT-12	211	2	9	34	45	1277	8376	9954	103	5	3	50	153	1672	7735	9721	2.3
AJT-15	2	0	17	3	97	1329	11,106	12,554	1	1	2	9	265	2162	10,844	13,284	5.5
AJT-17	4		2	3	96	590	356	1051	2		2	5	178	818	379	1384	24.1
AJT-14A		0			15	343	395	753	1	0	3	1	94	231	382	712	5.4
AJT-14B		1	2		21	562	460	1046	0	0	0		128	823	489	1440	27.4
AJT-21				1	44	316	256	617	0				85	457	253	795	22.4
AJT-22			0	1	33	154	162	350				1	98	152	176	427	18.0

4.3. Mineralogy and geochemistry of the mixed system downstream

Considering that in the dry season only the waste waters feed this branch of the stream, it is remarkable that the differences in water chemistry beyond the mixing zone in both seasons are less pronounced than would be expected (Fig. 3). Elemental concentrations in the waters are very similar in the first sampling point beyond the mixing zone for both seasons. However, there are slight differences that will be outlined briefly. In the dry season, element concentrations tend to be slightly lower, with the exception of SO_4^{2-} where a difference is not as evident. As the water moves towards the confluence with Ribeira do Rôxo the chemical trend observed is also very similar in both seasons. There is a gentle decrease in the concentration of As, and for Fe a similar trend is only clearly evident in the dry season. The unique case of As concentrations, apart from falling continuously in both seasons, is that in the summer they reach a value at the end of the path that is lower than its highest concentration past the mixing zone. Besides these slight differences, conductivity measurements remain constant in both seasons, and the pH tends to remain around 4 in the dry season and between 4.5 and 4.9 in the wet season, which is also a peculiar feature of the system.

The concentrations of the principal metals in the sediments, decrease to half or less of the initial, values with the notable exception of samples AJT-14A and AJT-14B for metals such as Cu and Zn. However, Pb values decrease one order of magnitude. As is also shown, most of these surficial sediments have high contents of Fe_2O_3, in particular both AJT-14 samples, but all samples beyond the mixing zone have Fe contents that are higher than samples collected closer to the mine waste piles, a feature that is worthy of note.

The major difference in sediment mineralogy downstream of the mixing zone is the absence of sulfide minerals, notably pyrite, a mineral still identified in the mixing zone. Few minerals are detectable by XRD apart from the detrital phases derived from the basement rock; hydroxysulfates dominate, especially jarosite, as shown by XRD. Nevertheless, hydroxysulfates commonly form hard crusts over dried rock surfaces exposed to the air during the summer. The XRD results suggest that sample AJT-21 may have Pb–jarosite, but its identification is ambiguous.

The continuous flow of municipal waste waters into the Ribeira da Água Forte delivers a mass of turbid grayish waters that turn into turbid yellowish waters a few tens of meters downstream. The surface of sediments and boulders typically becomes stained orange-red due to Fe oxyhydroxide precipitation. Some Fe oxyhydroxides are deposited over a frothy material, which evolves from an organic filamentous polymer probably resulting from dead biological material where strains of Fe-oxidizing bacteria were identified (Gonçalves et al., 2007; Pinto, 2007). This material is actually the major constituent of sample AJT-14A. These oxyhydroxides are mostly amorphous and thus none were detected in the diffractograms, but their importance can easily be seen in the chemical analyses. The diffraction pattern of sample AJT-14A is noisy and this is attributed to the presence of amorphous and poorly crystallized phases; the treatment of the sample with oxalic acid and ammonium oxalate improved the diffraction pattern considerably (Fig. 10). The identification of schwertmannite is a difficult task, and the treatment with ammonium oxalate is known to dissolve schwertmannite (Bigham and Nordstrom, 2000). Most peaks for schwertmannite (Bigham et al., 1994) appear in the diffractogram and both the broad 2.55 Å and 1.66 Å reflections are absent in the treated sample. Peaks at 5.11, 3.34 and 2.55 Å are compatible with the schwertmannite diffraction pattern presented by Bigham and Nordstrom (2000). It is worth noting that the diffraction pattern of the treated sample not only improved considerably but also has newer and sharper peaks

Please cite this article in press as: Maia, F., et al. Metal partitioning in sediments and mineralogical controls on the acid mine drainage in Ribeira da Água Forte (Aljustrel, Iberian Pyrite Belt, Southern Portugal). Appl. Geochem. (2012), http://dx.doi.org/10.1016/j.apgeochem.2012.02.036

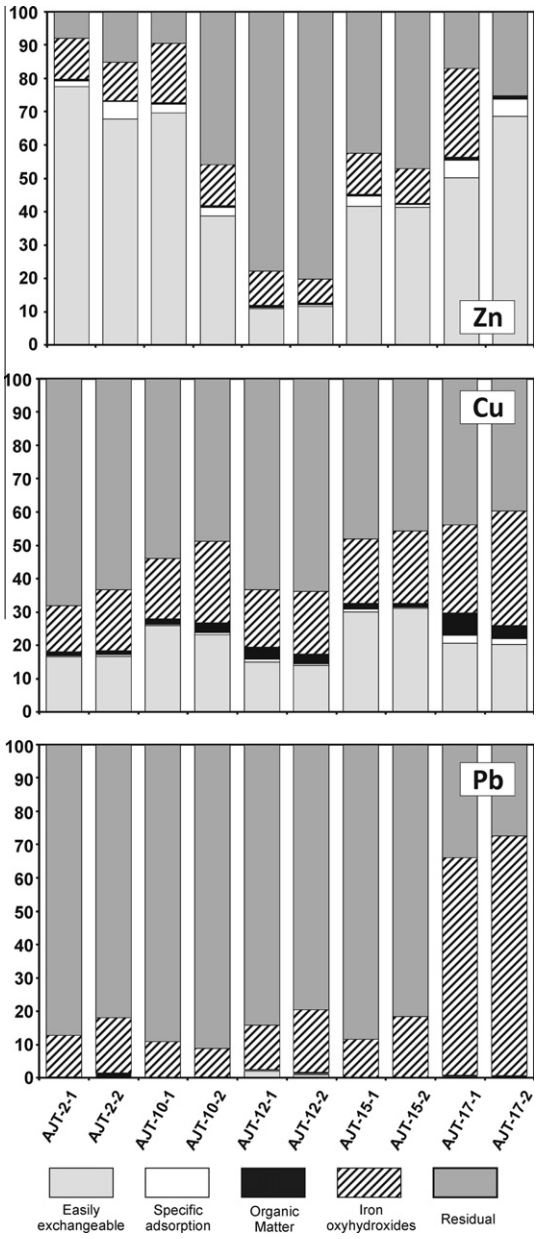

Fig. 7. Cumulative extraction (%) of Cu, Zn and Pb in the different steps for the set of samples up to the mixing zone. The sediment samples (labeled as 1 and 2) are put side-by-side for comparison as they represent the repeated extraction procedure of the same sample. Sediments are ordered as a function of distance from the mine waste rock piles along the Ribeira da Água Forte.

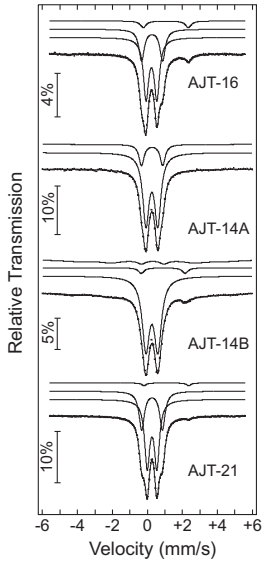

Fig. 8. Mössbauer spectra of sediment samples taken at 295 K. The lines over the experimental points are the sum of doublets, shown slightly shifted for clarity, corresponding to Fe atoms on different phases (see text and Table 4).

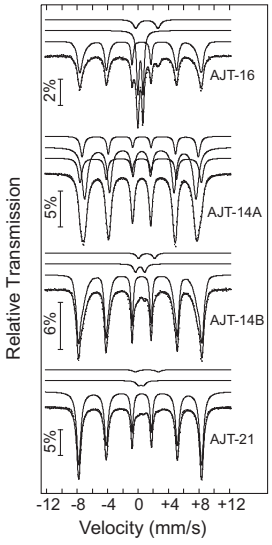

Fig. 9. Mössbauer spectra of sediment samples taken at 4 K. The lines over the experimental points are the sum of sextets or doublets, shown slightly shifted for clarity, corresponding to Fe atoms on different phases (see text and Table 4).

mostly being attributable to hydronium jarosite. Unlike samples AJT-4 and AJT-5, where dissolved sulfates reacted to produce crystalline oxalates after treatment with the oxalate solution, peaks of hydroxysulfate minerals, most of them attributable to hydronium jarosite (and jarosite in the untreated sample), were enhanced. The appearance of several new peaks in the oxalate treated sample suggests, as it happened with samples AJT-4 and AJT-5, that new phases have re-precipitated from a less stable, Fe-rich, poorly crystalline hydroxysulfate phase (schwertmannite). Also, the lack of any significant K in the sample suggests that the newly formed phase is most probably hydronium jarosite. Finally, the abundant presence of Fe oxyhydroxides and other Fe-bearing phases and their proper identification cannot be resolved with XRD alone.

In agreement with the XRD and geochemistry data, pyrite is not detected in the AJT-14A Mössbauer spectra (Fig. 8 and 9). The 295 K spectrum may be fitted with two doublets indicating the presence of jarosite in addition to the main contribution due to SPO. The 4 K spectrum is the sum of unresolved magnetic sextets. In this case it was not possible to analyze it as a single B_{hf} distribution. An attempt to fit this spectrum with three magnetic sextets with different IS, B_{hf} and quadrupole shifts led to the estimated parameters summarized in Table 4. A tentative assignment of these sextets can be proposed. The estimated parameters of the sextet with $B_{hf} \sim 47.3$ T are close to those reported for jarosite at 4 K (Murad, 1998; Bigham and Nordstrom, 2000) and the relative area is similar to that deduced for the jarosite doublet at 295 K. The remaining sextets may be attributed to SPO.

As in the case of AJT-16 the broad peaks of the magnetic sextets observed in the AJT-14B spectra at 295 and 4 K (Figs. 8 and 9) were fitted with a distribution of B_{hf}. In contrast to AJT-14A, in AJT-14B

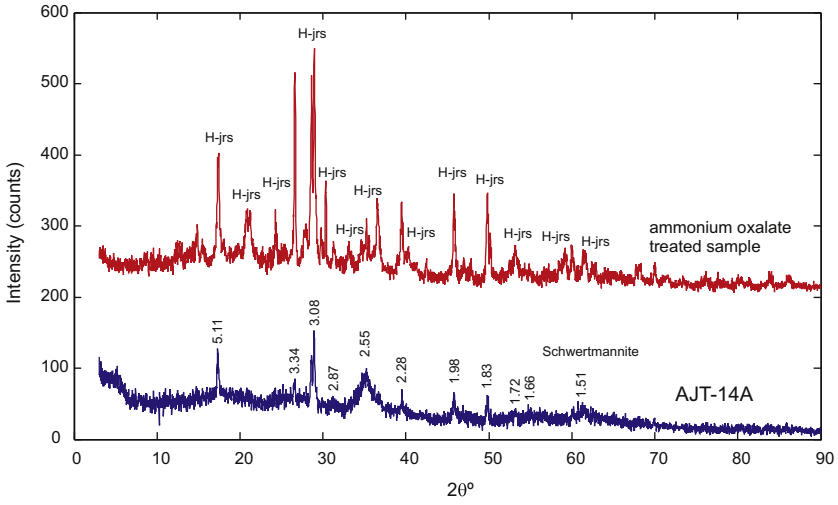

Fig. 10. X-ray diffractogram (Cu Kα) of sample AJT-14A; ammonium oxalate treated sample above shifted 200 units upward and untreated sample below. This sample shows distinctive behavior upon treatment as compared with sample AJT-4 (Fig. 5). Diffraction pattern of sample AJT-14A with the d-spacing of some relevant peaks, consistent with schwertmannite. The treated sample shows additional peaks, most of them attributable to hydronium jarosite (H-jrs) (see text for discussion).

no jarosite is detected. Most of the Fe is Fe^{3+} in SPO. The parameters of the doublet with small QS observed at 4 K show that it may not be assigned to pyrite. It may be consistent with Fe^{3+} in phyllosilicates. The Fe^{2+} in these phases is also identified. Because S-containing compounds are expected in the sample it may be tempting to attribute to schwertmannite, at least in part, the contributions with B_{hf} lower than 46 T (Murad, 1998; Bigham and Nordstrom, 2000) in the distribution of magnetic hyperfine fields fitted to the 4 K spectrum. A similar assignment could be proposed for AJT16 and AJT14A where sextets with $B_{hf} < 46$ T are also present. These contributions may be due to ferrihydrite (Bigham and Nordstrom, 2000), which is also likely present and even to dominate in these samples. Nevertheless, considering that XRD data strongly suggests the presence of schwertmannite in AJT-14A, sextets with $B_{hf} < 46$ T are at least in part due to this hydroxysulfate.

In AJT-21 (Fig. 8 and 9) there is a significant amount of jarosite. No sulfides were detected. The quadrupole doublet with smaller splitting present at 4 K has IS and QS significantly higher than those of pyrite at 4 K and closer to those of octahedrally coordinated Fe^{3+} in phyllosilicates (McCammon, 1995; Murad, 1998). The Fe^{2+} in phyllosilicates is also detected and most of the Fe is again present as Fe^{3+} in SPO.

In summary, the overall results from Mössbauer spectroscopy assert that the amount of jarosite gradually decreases from AJT-12 to AJT-16 and AJT-14A, is not detected at AJT14B, below the surface, then rises again at AJT-21. Pyrite is significant in AJT-12 and AJT-16 but is no longer detected at AJT-14 or AJT-21. The Fe^{2+} in phyllosilicates is always present but in small amounts. In all samples, Fe^{3+} in Fe oxides-oxyhydroxides dominates, except in AJT-12, where the highest fraction of Fe is present in jarosite.

Sequential extraction results show two major aspects of metal partitioning in this branch of the Ribeira da Água Forte (Fig. 11 and Table 5). Firstly, Cu is the only metal whose association with organic matter is significant, ranging from 2% to 8% of total metal content in the sediment, and in fact the high affinity of Cu for organic ligands is well known as extensively documented in waste waters and other environments (Cabaniss and Shuman, 1988; Ramos et al., 2002; Alvarez-Puebla et al., 2004; Gonçalves et al., 2004). In both AJT-14 samples, the amount of Cu extracted with organic matter was highest, and of the same magnitude as in sample AJT-17 collected at the mixing zone. This shows the peculiarity of the AJT-14 sediments, where the underlying darker sediment (AJT-14B), with no indication of having any sort of Fe sulfides as shown by Mössbauer spectroscopy and XRD, has a color that must be due to the accumulation of organic material, probably from the successive burying of the uppermost Fe-covered organic frothy material. Secondly, Fe oxyhydroxides are one of the most important phases for metal scavenging, an aspect which is clearly documented for the elements under study, and as the Mössbauer and XRD results seem to document the increase in the relative amounts of metals associated with Fe oxyhydroxides increase downstream of the mixing zone, being on the order of 60–70% for Pb, 50% for Cu, and 30–60% for Zn. Even considering that some hydroxysulfate minerals may also be dissolved in these steps, the much lower amounts in the samples do not affect the results in any significant way. As has been stressed before, these sediments have significant amounts of Fe oxyhydroxides, and it is extremely difficult to dissolve all these phases. For most sediments both steps for Fe-oxyhydroxide extraction were not fully efficient, and some sediments still showed their orange-yellow characteristic color (with a paler tone) after extraction steps E4A and E4B. The sequential extraction schemes used and published in the literature were optimized for samples with much less Fe than these samples, thus greater amounts of extractant solution must be used but with the undesirable effect of increasing the uncertainty in the final results. The use of multiple oxyhydroxide removal steps barely increases the extraction efficiency by more than 20%, as it was shown for very Fe-rich samples (Maia, 2010). Metal extraction from the residual phases showed some variations, but decreased in this branch of the stream. Again, Pb is very regular and the extraction pattern clearly differentiates the sediments collected upstream of the mixing zone from those collected downstream. However, because of the unknown extraction efficiency of Fe oxyhydroxides, the amounts extracted in the residual phases are merely indicative.

4.4. The chemical system of Ribeira da Água Forte

Acid-mine drainage in Aljustrel is still a serious problem for the Ribeira da Água Forte, because this stream receives effluent from the ancient mine dumps where the abandoned mine workings, the cementation pools and the acid–water pond are located. In spite of several remediation attempts in the past decade, the stream still shows its characteristic red color and very low pH. Ribeira da Água Forte is among the few streams that do not dry out completely along its length in the summer. Even though this

Please cite this article in press as: Maia, F., et al. Metal partitioning in sediments and mineralogical controls on the acid mine drainage in Ribeira da Água Forte (Aljustrel, Iberian Pyrite Belt, Southern Portugal). Appl. Geochem. (2012), http://dx.doi.org/10.1016/j.apgeochem.2012.02.036

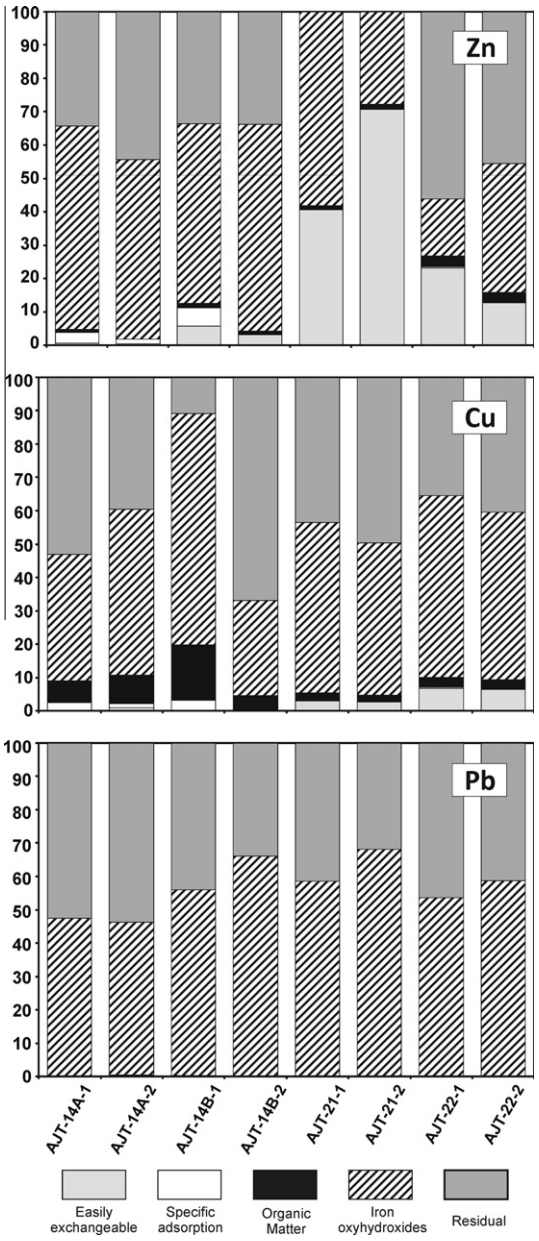

Fig. 11. Cumulative extraction (%) of Cu, Zn and Pb in the different steps for the set of samples downstream of the mixing zone. The sediment samples (labeled 1 and 2) are put side-by-side for comparison as they represent the repeated extraction procedure of the same sample. Sediments are ordered as a function of distance from the mine waste rock piles along the Ribeira da Água Forte.

characteristic results from human intervention, it is particularly useful for learning about the impacts of AMD in the area. As previously described, this AMD system can be separated into different segments in the path along the Ribeira da Água Forte, marked by the place where untreated municipal waste waters discharge into the stream and mix with the acid waters. Upstream of this mixing zone the stream behaves as typical acid drainage with waters of low pH (1.5–2.5), high Fe and SO_4^{2-} content, fairly high Ca and Mg, and a high load in trace elements such as Cu, Zn, As, Co, Cd, Ni and Ba. These waters show seasonal chemical variations as a consequence of changing rainfall frequency, resulting in dilution of the acid waters during the winter season. However, in the summer the stream dries up in this segment to the point when the acid water flow disappears except for several stagnant pools. As a consequence, metals concentrate in solution to the limit that induces the precipitation of several secondary minerals, such as gypsum and jarosite. These repeated cycles of flooding and dryness lead to the accumulation of these hydroxysulfates in the upper layers of the sediments, locally as crusts. The more soluble minerals are redissolved during the wetter season, but jarosite is less soluble and is known to be stable at a pH less than 3 and high SO_4^{2-} concentrations (Peretyazhko et al., 2009), thus remaining in the sediments. These cycles appear to be necessary for the accumulation of hydroxysulfate minerals and precipitation of Fe oxyhydroxides (identified as SPO by Mössbauer spectroscopy) in the sediments because even with the high element concentrations, the acid solution remains undersaturated in most sulfate minerals and amorphous $Fe(OH)_3$. These phases, and especially the Fe oxyhydroxides, are important metal scavengers but the high acidity of the waters is an inhibiting factor to cation adsorption because under such pH conditions most mineral surfaces are predominantly positively charged reducing considerably the number of surface sites where cations can bind. This is particularly critical for oxyhydroxides because the pH of their point of zero charge (pH_{pzc}), when the number of positive and negative surface charges is balanced, is typically around 8, but less so for most silicate surfaces with pH_{pzc} lying in the range between 2 and 5. Nevertheless, the amount of easily exchangeable Zn is significant in striking contrast with Cu, whereas the amount of Pb is negligible. Among the pool of elements, As may be an exception because it occurs predominantly as $H_2AsO_4^-$ species under these conditions favoring its adsorption. On the other hand Ba is probably fixed in the very insoluble barite although this mineral has not been detected by XRD. The remaining metals do not partition into the sediments in any significant way. Additionally, the high ionic strength of these waters also reduces the adsorption capacity of mineral surfaces. Therefore, under acid drainage conditions the capacity of natural system to mitigate these effects is low. Only Pb has comparatively low concentrations in the waters in spite of having very high concentration in the sediments. Along this segment of the Ribeira da Água Forte there is abundant pyrite that results from the transport of the very fine grained material from the mine dumps, and it remains unaltered buried in the sediments. No other sulfide minerals were detected apart from sphalerite in sample AJT-10.

The introduction of the organic-rich municipal waste waters directly into the Ribeira da Água Forte stream 2 km away from the mine dumps changes the chemistry of the system. However, this must be discussed in two different contexts because the mixture of the waters occurs only in the wetter rainy season.

4.4.1. Wet season

Under these flow conditions the pH of the acid waters after mixing with the waste waters is changed to 4.8 and the gradient of the waste-water source makes the mixing process turbulent. Sample AJTA-10-1 corresponds to this reduced, organic-rich water end member, having a pH of 8.4 when collected in the summer. These reduced conditions are able to preserve pyrite in the sediments, as shown in sediment samples AJT-16 and AJT-17, but there is no evidence of Fe sulfide precipitation under these conditions in this sample; the Mössbauer data detects only a minimum in the amount of jarosite in the sediments. Samples collected in this zone (AJT-16 and AJT-17), as in all other sites, were in accessible places that are normally under water only during the wetter season. The central and deeper part of the stream has not been sampled, and the extensive grassland area that develops some meters downstream may possibly develop the required conditions for reduced metal precipitation. However, knowledge of such processes in this zone is at present nonexistent. If there were significant metal sulfide precipitation under these conditions at the site of water sampling, the pH should not have dropped as much when the acid waters mix at this point.

Please cite this article in press as: Maia, F., et al. Metal partitioning in sediments and mineralogical controls on the acid mine drainage in Ribeira da Água Forte (Aljustrel, Iberian Pyrite Belt, Southern Portugal). Appl. Geochem. (2012), http://dx.doi.org/10.1016/j.apgeochem.2012.02.036

As previously mentioned in Section 4.2, the resulting water in the mixing zone can be viewed as a mixture of sample AJTA-9-2 with a water mass whose composition should approach the composition of sample AJTA-10-1 (but more dilute). Inverse models were tested in order to obtain the composition of water sample AJTA-10-2 from the two previous samples. However, because the uncertainties used were rather large the results should be considered with caution. Nevertheless, it is remarkable that the most consistent models, which considered a range of 10 to 40% dilution of sample AJTA-10-1 with water in equilibrium with the atmosphere, indicate that a mixture of about 80% of the municipal waste water with 20% of the acid water, jointly with Fe oxyhydroxide precipitation and hydroxysulfate dissolution is required to grossly match the chemical composition of sample AJTA-10-2. Iron oxyhydroxide precipitation is very likely under these mixing conditions, because the Fe concentration in the acid water is substantial, and the sudden mixing with the high pH waste water immediately results in a solution supersaturated with amorphous Fe hydroxide. Such mixture volumes were not measured in the field but the flux of municipal waste water when it was sampled in March 2007 greatly surpassed the flux of acid water coming from the mining waste piles along the Ribeira da Água Forte. What these calculations show is that the concentration pattern that is observed cannot be solely explained considering a simple mixture of waters. Therefore, the agreement with the previous calculations using conservative elements is highly supportive of such mixing ratios which seem appropriate to describe the flow water system in Ribeira da Água Forte at the time of sampling. Additionally, both Fe oxyhydroxide precipitation and their surface affinity to adsorb As in these conditions may also explain the overestimation of Fe and As concentrations in the resulting mixture (Section 4.2). A gentle attenuation of metal concentration in solution, that has limited impact in the range of concentrations observed, occurs downstream. However, the continuous decrease in As concentration means that adsorption of As, especially on Fe oxyhydroxides surfaces must be an important mechanism at work, and Fe concentration is also reduced by more than 50%, unlike SO_4^{2-} which remains more or less constant. Waters are normally undersaturated relative to most important minerals, with the exception of barite and gypsum, thus suggesting the importance that the successive wet/dry cycles have on mineral precipitation and accumulation in the sediments.

4.4.2. Dry season

The situation that develops in the dry season is very important because even though the metal input from the acid waters is interrupted, metal concentrations in the waters downstream of the mixing zone rapidly rise to values not much different from those obtained during the wetter season. The jump in concentration in all elements is quite remarkable from sample AJTA-10-1 to AJTA-8-1, especially for Fe and SO_4^{2-}. This suggests that the highly reduced, organic-rich, and high pH municipal waste waters are distinctly out of equilibrium with the secondary mineralogy in the sediments, especially Fe oxyhydroxides and hydroxysulfate minerals. Unlike the previous situation, there is no mixing of waters and coupled dissolution/precipitation of these phases in response to changing chemical conditions is very likely. As a result, transition metals adsorbed or incorporated on the phases being dissolved are immediately released. The association of Zn, Cu, and Pb with oxyhydroxide phases has been demonstrated and supports the plausibility of this mechanism. Even Co, Cd and Ni, which apparently seem to interact very little with the sediment mineral phases must be associated with this secondary mineralogy, otherwise it would be hard to explain their slight increase in concentration. The sediments in this zone show the presence of pyrite, jarosite and small Fe^{3+} oxyhydroxide (SPO) particles. Furthermore, schwertmannite can be formed at a pH between 3 and 4 (Bigham et al., 1994). Minerals from the jarosite group are less soluble than most other Fe sulfates, which allow them to be preserved in the sediments. However, jarosite can become increasingly unstable under high pH low Eh environments due to reduction of Fe^{3+} as is observed in inundated acid sulfate soils (Keene et al., 2010). Iron hydroxysulfate minerals also play a fundamental role in AMD systems, because both their precipitation and dissolution followed by transformation into more stable Fe hydroxide releases acidity, a phenomenon well documented in several AMD systems (Bigham and Nordstrom, 2000; Peretyazhko et al., 2009). Considering the reaction of schwertmannite dissolution:

$$Fe_8O_8(OH)_6(SO_4) + 22H^+ = 8Fe^{3+} + SO_4^{2-} + 14H_2O, \quad (3)$$

the Fe^{3+} released is immediately precipitated from solution by the reaction:

$$Fe^{3+} + 3H_2O = Fe(OH)_3 + 3H^+. \quad (4)$$

The net effect is an increase in acidity. Sulfur content in the sediments immediately upstream and downstream of the mixing waters zone is in the order of 6 wt.%, and in sample AJT-17 is only 2 wt.%. Therefore, it is very likely that SO_4 reductive dissolution is occurring in this environment and jarosite is the best candidate because of its abundance in these sediments. As mentioned above in Section 4.3, the turbid waters rapidly turn a yellowish color, which results from Fe^{3+} in the suspended load that gradually settles along the stream until they become clear at about 2.5 km further downstream. The best evidence obtained for the presence of schwertmannite is observed downstream on this path in sample AJT-14A. Bigham et al. (1990) reported the formation of a poorly crystallized Fe oxyhydroxysulfate, later identified as schwertmannite (Bigham et al., 1994), by Fe oxidizing bacteria in a pH range of 3–4.5. Such Fe oxidizing bacteria have been identified in this site (Gonçalves et al., 2007; Pinto, 2007) and pH values in the drier season were around 4 at the site of AJT-14A sample. Furthermore, the S content of the sample is in the order of 6.5 wt.%. Therefore, in spite of Mössbauer spectra being inconclusive, the XRD data supports the existence of schwertmannite in this sample and most likely in the stream sediments between the mixing zone and this site. Mössbauer data also show that sulfate minerals (jarosite) are no longer detected in sample AJT-14B, and Fe^{3+} is mostly attributable to SPO. This suggests that, because of the transient nature of the Fe hydroxysulfate in sample AJT-14A, it gradually transforms into Fe oxyhydroxides during the burial of the sediment, a feature well documented for schwertmannite (Bigham et al., 1994, 1996; Knorr and Blodau, 2007; Burton et al., 2008; Peretyazhko et al., 2009). Sulfur content is also clearly lower than in sample AJT-14A, but equivalent to AJT-21, where jarosite is detected again. Because Mössbauer hyperfine parameter values of schwertmannite are within the range of those of SPO, this supports the plausibility of schwertmannite presence in these samples. Therefore, the coupled interplay of reactions (3) and (4) can generate the acidity that is required to lower the pH from the 8.4 measured in the waste water to 4 at the site of samples AJT-14, and to 3.9 in the site of sample AJT-21, almost 6 km distant from the mixing zone. In these sediments, SPO dominates and jarosite increases in AJT-21. The abundant small particles of Fe^{3+} oxyhydroxides control metal (Cu, Zn and Pb) content in the sediments, especially Pb, even if important amounts of these metals have been shown to be extracted in the residual phase step. As was previously observed, the amounts of SPO in the samples make it difficult to quantify the efficiency of the corresponding sequential extracting steps. Nevertheless, the SPO seems to be responsible for the slight decrease of these metals in solution, even for the elements Co, Ni and Cd. However, none of these metal concentrations in solution actually recover from the initial release of chemical elements that

Please cite this article in press as: Maia, F., et al. Metal partitioning in sediments and mineralogical controls on the acid mine drainage in Ribeira da Água Forte (Aljustrel, Iberian Pyrite Belt, Southern Portugal). Appl. Geochem. (2012), http://dx.doi.org/10.1016/j.apgeochem.2012.02.036

takes place with the input of the waste water. The notable exception is As. All other elements thus enter the Ribeira do Rôxo stream still having very high concentrations in solution.

5. Conclusions

The chemical characteristics of the Ribeira da Água Forte along its flow path, both from the flowing waters and stream sediments, reveal a system from which some lessons can be learned with respect to the impact of AMD and potential mitigation procedures. After decades of intense mining, the impacts are visible everywhere. Recent intervention and reclamation over the main mine tailings near the town of Aljustrel have helped to minimize some impacts but have not remedied the persistence of AMD conditions along the Ribeira da Água Forte. The current reality is that the municipal waste waters collected in pools overflow throughout the year towards the Ribeira da Água Forte inducing geochemical processes that have not been controlled since it started. None of these processes has been properly studied and assessed, and thus, little was known about the chemistry and mechanisms that operate in this system. The results obtained in this study help shed light on these processes. Therefore, the geochemical processes taking place along the Ribeira da Água Forte are summarized as follows:

1. Typical AMD conditions develop along the first 2 km in the Ribeira da Água Forte and chemical variations in the stream waters are primarily controlled by seasonal cycles of flooding and drying of the stream bed. The flowing waters are correspondingly diluted and concentrated, inducing the precipitation of efflorescent sulfate minerals and amorphous Fe oxyhydroxides in the dry season. Less stable secondary minerals are redissolved but some, such as jarosite, accumulate in the stream sediments. Despite active weathering conditions prevailing in the system, pyrite (and minor sphalerite) are preserved in these same sediments.
2. At the time of sampling in the mixing zone, an estimated volume of 20% acid water mixed with 80% municipal waste water in a turbulent process. Whereas most element concentrations in the mixed water can be explained by a conservative mixing process (no gains and/or losses), Fe and As behave differently because Fe oxyhydroxide precipitation occurs with subsequent As adsorption. Furthermore, a simple conservative mixture would require a different acid water to waste water mixing ratio (1:3) to match the measured pH, and such a mixing ratio does not fit any of the inverse models calculated.
3. In the wet season, the flowing water downstream of the mixing zone does not change its chemistry significantly. The Fe concentration is slightly reduced along the flow path while As maintains its decreasing trend until it reaches a minimum concentration of tens of μg/L in solution. The attenuating mechanisms are the same as discussed earlier.
4. The dry season is characterized by totally different conditions because the waste water is the only water input for the Ribeira da Água Forte from the mixing zone downstream. This reduced, organic-rich, and high pH water promotes the reductive dissolution of both Fe oxyhydroxide and hydroxysulfates of the stream sediments in the mixing zone. Consequently, metals and other trace elements are released into solution up to a level equivalent to the concentrations observed in the next sampling point during the wet season with the contribution of the acid-drainage waters.
5. There is significant Fe oxyhydroxide precipitation in the dry season, revealed by the clear reduction of Fe in solution along the flow path, and by the occurrence of greater amounts of small particle Fe oxyhydroxides in these sediments. Additionally, evidence was gathered of schwertmannite formation in sediments downstream of the mixing zone for a few kilometers. Both Fe hydroxide precipitation and schwertmannite transformation sustain the reduction of the pH from the initial 8.4 to 3.9 – 4.2 downstream, values that are even lower than in conditions when both waters mix during the wet season.
6. Metals in solution show the same trend as during the wet season with only little differences. Like all other elements As is released into solution at the mixing zone but it is the only element whose concentration is reduced to levels below its initial value along the stream path.
7. Distribution of Cu, Zn and Pb in the sediments is heterogeneous, but they are predominantly associated with Fe oxyhydroxides and/or residual phases. Despite this association, the capacity of the newly formed phases to reduce the concentration of these metals in solution is limited.

The final outcome of these processes throughout the year is high metal concentrations in the waters arriving at Ribeira do Rôxo at best varying within only an order of magnitude between the wet and dry seasons. It is misleading to consider the waste water input as a mitigating mechanism because this reduced high pH water represents a reacting medium that is in disequilibrium with the stream sediment secondary mineralogy. Therefore, a permanent metal-releasing mechanism to the stream is sustained, developing an equally deleterious situation that is difficult to remediate.

Acknowledgements

The authors wish to express their gratitude to the detailed review of Associate Editor Dr. Robert Seal and two anonymous referees, which improved the current manuscript considerably. This work is a contribution from Project METALTRAVEL – POCI/CTE-GEX/61700/2004, funded by MCTES-FCT, Portugal.

References

Abreu, M.M., Figueiredo, M.O., Waerenborgh, J.C., Cabral, J.M.P., 1988. Oriented overgrowth of acicular maghemite crystals on quartz. Clay Min. 23, 357–365.
Acero, P., Ayora, C., Torrentó, C., Nieto, J.M., 2006. The behaviour of trace elements during schwertmannite precipitation and subsequent transformation into goethite and jarosite. Geochim. Cosmochim. Acta 70, 4130–4139.
Alvarez-Puebla, R.A., Valenzuela-Calahorro, C., Garrido, J.J., 2004. Cu(II) retention on a humic substance. J. Colloid Interface Sci. 270, 47–55.
Barriga, F.J.A.S., Carvalho, D., 1983. Carboniferous volcanogenic mineralization in South Portugal (Iberian Pyrite Belt). Mem. Serv. Geol. Portugal 29, 99–116.
Barriga, F.J.A.S., Fyfe, W.S., 1998. Multi-phase water–rhyolite interaction and ore fluid generation at Aljustrel, Portugal. Mineral. Depos. 33, 188–207.
Bermond, A., 2001. Limits of sequential extraction procedures re-examined with emphasis on the role of H^+ ion reactivity. Anal. Chim. Acta 445, 79–88.
Bigham, J.M., Nordstrom, D.K., 2000. Iron and aluminum hydroxysulfates from acid sulfate waters. In: Alpers, C.N., Jambor, J.L., Nordstrom, D.K. (Eds.), Sulfate Minerals. Reviews in Mineralogy and Geochemistry, vol. 40 (Chapter 7).
Bigham, J.M., Schwertmann, U., Carlson, L., Murad, E., 1990. A poorly crystallized oxyhydroxysulfate of iron formed by bacterial oxidation of Fe(II) in acid mine waters. Geochim. Cosmochim. Acta 54, 2743–2758.
Bigham, J.M., Carlson, L., Murad, E., 1994. Schwertmannite, a new iron oxyhydroxysulfate from Pyhäsalmi, Finland, and other localities. Mineral. Mag. 58, 641–648.
Bigham, J.M., Schwertmann, U., Traina, S.J., Winland, R.L., Wolf, M., 1996. Schwertmannite and the chemical modeling of iron in acid sulfate waters. Geochim. Cosmochim. Acta 60, 2111–2121.
Breward, N., Williams, M., Bradley, D., 1996. Comparison of alternative methods for determining particulate metal fractionation in carbonate-rich Mediterranean soils. Appl. Geochem. 11, 101–104.
Burton, E.D., Bush, R.T., Sullivan, L.A., Mitchell, D.R.G., 2008. Schwertmannite transformation to goethite via the Fe(II) pathway: reaction rates and implications for iron sulfide formation. Geochim. Cosmochim. Acta 72, 4551–4564.
Cabaniss, S.E., Shuman, M.S., 1988. Copper binding by dissolved organic matter: I. Suwannee River fulvic acid equilibria. Geochim. Cosmochim. Acta 52, 185–193.

Carvalho, C.M.N., 1998. Zonas de alteração hidrotermal associadas aos depósitos de sulfuretos maciços da Faixa Piritosa Ibérica: Estudo difractométrico dos filossilicatos que as caracterizam. MSc Thesis, Dep. Geologia, Faculdade de Ciências da Universidade de Lisboa.

Carvalho, D., 1976. Considerações sobre o vulcanismo da região Cercal-Odemira: suas relações com a Faixa Piritosa Ibérica. Comun. Serv. Geol. Portugal 60, 216–238.

Carvalho, D., Barriga, F.J.A.S., Munhá, J., 1999. Bimodal siliciclastic systems – the case of the Iberian Pyrite Belt. In: Barrie, C.T., Hannington, M. (Eds.), Reviews in Economic Geology, vol. 8, pp. 375–408.

Cheetam, A.K., Cole, A.J., Long, G.J., 1981. Investigation of the mixed-metal sulfide (Mn, Fe)S2 by analytical electron microscopy and Mössbauer spectroscopy. Inorg. Chem. 20, 2747–2750.

Coey, J.M.D., 1988. Magnetic properties of iron in soil iron oxides and clay minerals. In: Stucky, J.W., Goodman, B.A., Schwertmann, U. (Eds.), Iron in Soils and Clay Minerals, Nato ASI Series C, vol. 217. D. Reidel Publ. Co., Dordrecht, pp. 397–466 (Chapter 14).

Druschel, G.K., Baker, B.J., Gihring, T.M., Banfield, J.F., 2005. Acid mine drainage biogeochemistry at Iron Mountain, California. Geochem. Trans. 5, 13–32.

Figueiras, J., Waerenborgh, J.C., 1997. Fully oxidized chromite in the Serra Alta (South Portugal) quartzites: chemical and structural characterization and geological implications. Mineral. Mag. 61, 627–638.

Finklea III, S.L., Cathey, Le Conte, Amma, E.L., 1976. Investigation of the bonding mechanism in pyrite using the mossbauer effect and X-ray crystallography. Acta Cryst. A32, 529–537.

Galán, E., Gómez-Ariza, J.L., González, I., Fernández-Caliani, J.C., Morales, E., Giráldez, I., 2003. Heavy metal partitioning in river sediments severely polluted by acid mine drainage in the Iberian Pyrite Belt. Appl. Geochem. 18, 409–421.

Gonçalves, M.A., Nogueira, J.M.F., Figueiras, J., Putnis, C.V., Almeida, C., 2004. Basemetals and organic content in stream sediments in the vicinity of a landfill. Appl. Geochem. 19, 137–151.

Gonçalves, M.A., Figueiras, J., Pinto, C., Neng, N., Sá-Pereira, P., Batista, M.J., 2007. Biogeochemical and mineralogical characteristics of the acid mine drainage system in Aljustrel and S. Domingos mines, Iberian Pyrite Belt. Geochim. Cosmochim. Acta 71, A341.

Grimalt, J.O., Ferrer, M., MacPherson, E., 1999. Special issue: the mine tailing accident in Aznalcollar. Sci. Total Environ. 242, 3–11.

Hirner, A.V., 1992. Trace element speciation in soils and sediments using sequential chemical extraction methods. Int. J. Environ. Anal. Chem. 46, 77–85.

Hirner, A.V., 1996. Testing metal mobility in soils by elution tests. In: Reuther, R. (Ed.), Geochemical Approaches to Environmental Engineering of Metals. Springer, pp. 15–23.

Hubbard, C.G., Black, S., Coleman, M.L., 2009. Aqueous geochemistry and oxygen isotope compositions of acid mine drainage from the Río Tinto, SW Spain, highlight inconsistencies in current models. Chem. Geol. 265, 321–334.

Keene, A., Johnston, S., Bush, R., Sullivan, L., Burton, E., 2010. Reductive dissolution of natural jarosite in a tidally inundated acid sulfate soil: geochemical implications. In: Proc. 19th World Congress of Soil Science, Soil Solutions for a Changing World, 1–6 August 2010, Brisbane, Australia, pp. 100–103.

Kheboian, C., Bauer, C.F., 1987. Accuracy of selective extraction procedures for metal speciation in model aquatic sediments. Anal. Chem. 59, 1417–1423.

Knorr, K.-H., Blodau, C., 2007. Controls on schwertmannite transformation rates and products. Appl. Geochem. 22, 2006–2015.

Kretz, R., 1983. Symbols of rock-forming minerals. Am. Mineral. 68, 277–279.

Maia, F.M.S., 2010. Adsorção de cobre em matrizes naturais provenientes de depósitos do tipo raña. MSc Thesis, Dep. Geologia, Faculdade de Ciências da Universidade de Lisboa.

McCammon, C.A., 1995. Mössbauer spectroscopy of minerals. In: Ahrens, T.J. (Ed.), Mineral Physics and Crystallography: a Handbook of Physical Constants. Amer. Geophys. Union, pp. 332–347.

Morillo, J., Usero, J., Gracia, I., 2002. Partitioning of metals in sediments from the Odiel River (Spain). Environ. Int. 28, 263–271.

Murad, E., 1988. Properties and behaviour of Fe oxides as determined by Mössbauer spectroscopy. In: Stucki, J.W., Goodman, B.A., Schwertmann, U. (Eds.), Iron in Soils and Clay Minerals, NATO ASI Series C, vol. 217. D. Reidel Publ. Co., Dordrecht, pp. 309–350 (Chapter 12).

Murad, E., 1998. Clays and clay minerals: what can Mössbauer spectroscopy do to help understand them? Hyperfine Interact. 117, 39–70.

Nordstrom, D.K., Alpers, C.N., 1999. Negative pH, efflorescent mineralogy, and consequences for environmental restoration at the Iron Mountain Superfund site, California. Proc. Natl. Acad. Sci. USA 96, 3455–3462.

Nordstrom, D.K., Southam, G., 1997. Geomicrobiology of sulfide mineral oxidation. In: Banfield, J.F, Nealson, K.H. (Eds.), Geomicrobiology: Interactions Between Microbes and Minerals, Reviews in Mineralogy, vol. 35, pp. 361–190.

Oliveira, J.T., 1990. South Portuguese zone. In: Dallmeyer, R.D., Martinez Garcia, E. (Eds.), Pre-Mesozoic Geology of Iberia. Springer, Berlin, Heidelberg, New York, pp. 333–346.

Parkhurst, D.L., Appelo, C.A.J., 1999. User's guide to PHREEQC (Version 2) – a computer program for speciation, batch-reaction, one-dimensional transport, and inverse geochemical calculations. US Geol. Surv. Water-Resour. Invest. Rep. 99-4259.

Peretyazhko, T., Zachara, J.M., Boily, J.-F., Xia, Y., Gassman, P.L., Arey, B.W., Burgos, W.D., 2009. Mineralogical transformations controlling acid mine drainage chemistry. Chem. Geol. 262, 169–178.

Pérez-López, R., Nieto, J.M., Almodóvar, G.R., 2007. Immobilization of toxic elements in mine residues derived from mining activities in the Iberian Pyrite Belt (SW Spain): laboratory experiments. Appl. Geochem. 22, 1919–1935.

Pérez-López, R., Álvarez-Valero, A.M., Nieto, J.M., Sáez, R., Matos, J.X., 2008. Use of sequential extraction procedure for assessing the environmental impact at regional scale of the São Domingos Mine (Iberian Pyrite Belt). Appl. Geochem. 23, 2342–2346.

Pérez-López, R., Delgado, J., Nieto, J.M., Márquez-García, B., 2010. Rare earth element geochemistry of sulphide weathering in the São Domingos mine area (Iberian Pyrite Belt): a proxy for fluid–rock interaction and ancient mining pollution. Chem. Geol. 276, 29–40.

Pinto, C., 2007. Caracterização geoquímica das fases aquosas e sólidas associadas aos processos geradores de Drenagem ácida de minas (DAM), na zona envolvente às Minas de Aljustrel. MSc Thesis, Dep. Geologia, Faculdade de Ciências da Universidade de Lisboa.

Quevauviller, P., Rauret, G., Muntau, H., Ure, A.M., Rubio, R., López-Sanchez, J.F., Fiedler, H.D., Griepink, B., 1994. Evaluation of a sequential extraction procedure for the determination of extractable trace metal contents in sediments. Fresenius J. Anal. Chem. 349, 808–814.

Ramos, M.A., Fiol, S., López, R., Antelo, J.M., Arce, F., 2002. Analysis of the effect of pH on Cu^{2+} – fulvic acid complexation using a simple electrostatic model. Environ. Sci. Technol. 36, 3109–3113.

Sahuquillo, A., López-Sánchez, J.F., Rubio, R., Rauret, G., Thomas, R.P., Davidson, C.M., Ure, A.M., 1999. Use of a certified reference material for extractable trace metals to assess sources of uncertainty in the BCR three-stage sequential extraction procedure. Anal. Chim. Acta 382, 317–327.

Sánchez-España, J., López-Pamo, E., Santofimia, E., Aduvire, O., Reyes, J., Barettino, D., 2005. Acid mine drainage in the Iberian Pyrite Belt (Odiel river watershed, Huelva, SW Spain): geochemistry, mineralogy and environmental implications. Appl. Geochem. 20, 1320–1356.

Sánchez-España, J., López-Pamo, E., Santofimia-Pastor, E., Diez-Ercilla, E., 2008. The acidic mine pit lakes of the Iberian Pyrite Belt: an approach to their physical limnology and hydrogeochemistry. Appl. Geochem. 23, 1260–1287.

Schermerhorn, L.J.G., Zbyszewski, G., Ferreira, O.V., 1987. Mapa Geológico e Notícia Explicativa da Folha 42-D Aljustrel, Serviços Geológicos de Portugal.

Tessier, A., Campbell, P.G.C., Bisson, M., 1979. Sequential extraction procedure for the speciation of particulate trace metals. Anal. Chem. 51, 844–851.

Tovar-Sanchez, A., Huerta-Diaz, M.A., Negro, J.J., Bravo, M.A., Sañudo-Wilhelmy, S.A., 2006. Metal contamination in interstitial waters of Doñana Park. J. Environ. Manage. 78, 286–293.

Vandenberghe, R.E., Barrero, C.A., da Costa, G.M., Van San, E., De Grave, E., 2000. Mössbauer characterization of iron oxides and (oxy)hydroxides: the present state of the art. Hyperfine Interact. 126, 247–259.

Whitney, D.L., Evans, B.W., 2010. Abbreviations for names of rock-forming minerals. Am. Mineral. 95, 185–187.

Please cite this article in press as: Maia, F., et al. Metal partitioning in sediments and mineralogical controls on the acid mine drainage in Ribeira da Água Forte (Aljustrel, Iberian Pyrite Belt, Southern Portugal). Appl. Geochem. (2012), http://dx.doi.org/10.1016/j.apgeochem.2012.02.036